

## On the orbital forcing of Martian water and CO<sub>2</sub> cycles: A general circulation model study with simplified volatile schemes

Michael A. Mischna,<sup>1</sup> Mark I. Richardson,<sup>2</sup> R. John Wilson,<sup>3</sup> and Daniel J. McCleese<sup>4</sup>

Received 21 January 2003; revised 9 April 2003; accepted 30 April 2003; published 27 June 2003.

[1] Variations in the Martian water and CO<sub>2</sub> cycles with changes in orbital and rotational parameters are examined using the Geophysical Fluid Dynamics Laboratory Mars General Circulation Model. The model allows for arbitrary specification of obliquity, eccentricity, and argument of perihelion as well as the position and thickness of surface ice. Exchange of CO<sub>2</sub> between the surface and atmosphere is modeled, generating seasonal cycles of surface ice and surface pressure. Water is allowed to exchange between the surface and atmosphere, cloud formation is treated, and both cloud and vapor are transported by modeled winds and diffusion. Exchange of water and CO<sub>2</sub> with the subsurface is not allowed, and radiative effects of water vapor and clouds are not treated. The seasonal cycle of CO<sub>2</sub> is found to become more extreme at high obliquity, as suggested by simple heat balance models. Maximum pressures remain largely the same, but the minima decrease substantially as more CO<sub>2</sub> condenses in the more extensive polar night. Vapor and cloud abundances increase dramatically with obliquity. The stable location for surface ice moves equatorward with increasing obliquity, such that by 45° obliquity, water ice is stable in the tropics only. Ice is not spatially uniform, but rather found preferentially in regions of high thermal inertia or high topography. Eccentricity and argument of perihelion can provide a second-order modification to the distribution of surface ice by altering the temporal distribution of insolation at the poles. Further model simulations reveal the robustness of these distributions for a variety of initial conditions. Our findings shed light on the nature of near-surface, ice-rich deposits at midlatitudes and low-latitudes on Mars.

*INDEX TERMS:* 6225 Planetology: Solar System Objects: Mars; 5407 Planetology: Solid Surface Planets: Atmospheres—evolution; 5409 Planetology: Solid Surface Planets: Atmospheres—structure and dynamics; 5445 Planetology: Solid Surface Planets: Meteorology (3346); 0343 Atmospheric Composition and Structure: Planetary atmospheres (5405, 5407, 5409, 5704, 5705, 5707); *KEYWORDS:* Mars, Martian climate, obliquity, Mars GCM, surface ice, surface layering

**Citation:** Mischna, M. A., M. I. Richardson, R. J. Wilson, and D. J. McCleese, On the orbital forcing of Martian water and CO<sub>2</sub> cycles: A general circulation model study with simplified volatile schemes, *J. Geophys. Res.*, 108(E6), 5062, doi:10.1029/2003JE002051, 2003.

### 1. Introduction

[2] The existence of Polar Layered Deposits (PLD) and volatile-rich deposits at lower latitudes on Mars provide the tantalizing possibility that a detailed record of Martian climate variability has been written and now awaits our inspection. Spacecraft observations of the Red Planet by Mariner 9 and Viking detailed the highly stratiform nature of the PLD in both the northern and southern hemisphere.

Such terrain is expressed in two distinct forms. At higher latitudes, the PLD are comprised of a mixture of water ice and dust, with the layering a result of either alternating ice and dust layers, or layers of an ice-dust mixture with varying dust amounts in individual layers. The latest observations by Mars Global Surveyor (MGS) show these layers to be spatially distinct to the limiting resolution (1.4m) of the Mars Orbiter Camera (MOC). Slightly equatorward of the icy deposits in the southern hemisphere are similar layered terrains, the near-subsurfaces of which have been fully desiccated, but still retain the layered structure characteristic of PLD. Conventional thinking that such regions must have once been covered by surface or near-surface ground ice, perhaps during recent periods of obliquity excursion, and that they still retain substantial amounts of water ice just below the surface, has recently been confirmed by Mars Odyssey Gamma Ray Spectrometer/Neutron Spectrometer data [*Feldman et al.*, 2002; *Mitrofanov et*

<sup>1</sup>Department of Earth and Space Sciences, University of California, Los Angeles, Los Angeles, California, USA.

<sup>2</sup>Division of Geological and Planetary Sciences, California Institute of Technology, Pasadena, California, USA.

<sup>3</sup>Geophysical Fluid Dynamics Laboratory, Princeton, New Jersey, USA.

<sup>4</sup>Jet Propulsion Laboratory, Pasadena, California, USA.

*al.*, 2002; *Boynton et al.*, 2002]. These observations show substantial near-surface ground ice extending to 60° latitude in each hemisphere.

[3] It is widely accepted that volatile cycling on Mars is an active and important player in climate evolution. The transport of both carbon dioxide and water to and from the polar regions and low-latitudes both follows orbital forcing and causes significant climate change. It was first suggested by *Jakosky and Carr* [1985] that during periods of high obliquity, polar surface ice would be sublimed and transported away from the summer hemisphere polar cap and to the equatorial region, where it would be deposited, forming a perennial ice “belt”. The rate at which such a belt would be formed depends on the flux of water vapor from each polar cap during its respective summer, which itself depends on the vapor gradient from pole to equator, and such dynamical considerations as wind speed and turbulent mixing. On the basis of their best-case simulations, at present obliquity, only 1–100  $\mu\text{m}$  are sublimed annually, and the atmosphere remains saturated only in the high latitudes. In the tropics, the atmosphere falls well below the saturation vapor pressure, and so surface ice is unstable. As obliquity is increased, however, cap temperatures rise, placing considerably more water vapor into the atmosphere—up to 5000  $\mu\text{m}$  at 45° obliquity. The polar regions again reach saturation, but the annual transport of water from pole to (the now cooler) equator results in the deposition of ice in the oversaturated tropics. Rather than returning to the pole during winter, the tropical ice is “trapped” since sublimation is restricted due to the influx of vapor from the other hemisphere the following season.

[4] A set of papers by *Jakosky et al.* [1993, 1995] used a 1-D thermal model of the Martian poles to understand the seasonal transport of water ice over the past  $10^7$  years, while considering the influence of periodic changes in Martian obliquity and secular precession of the argument of perihelion (this determines the seasonal date at which perihelion occurs, where the seasonal indicator on Mars is  $L_s$ , an angular measure of season, with  $L_s = 0^\circ$  defined as northern spring equinox). Models of Martian orbit and spin parameters suggest that they can vary over a wider range than those of the Earth [*Ward and Rudy*, 1992]. Within the past 10 million years, these models suggest obliquity has varied from 15° to 45°. On longer timescales, the chaotic character of the obliquity eliminates the possibility of developing a precise history of obliquity, but suggests excursions from zero to 60° obliquity [*Touma and Wisdom*, 1993; *Laskar and Robutel*, 1993]. The goal of *Jakosky et al.* [1993, 1995] was twofold: to explain the difference in polar water ice deposit size (at the time it was thought that the south polar deposits were several times smaller than their northern counterpart) and to explain the discrepancy between orbital forcing mechanisms and the seasonal timescale for producing the individual layers inferred from models of the current water cycle [*Jakosky*, 1983a, 1983b; *Haberle and Jakosky*, 1990]. Their findings indicate a steady transfer of water vapor from the south pole to the north pole over the past 10 million years, which they suggest is a result of the difference in elevation between the higher southern and lower northern caps. This lopsided transfer continues until the reduced southern cap

size brings south to north flux in balance with the much weaker north to south flux. Also, their findings reveal that at high obliquity (>45°), very rapid sublimation of the polar caps could take place—on a timescale much quicker than either perihelion precession or obliquity change. This water vapor would preferentially deposit in the tropics, as explained above.

[5] The benefit of orbital parameter models of Martian volatile distribution is that they can explain the growth of the PLD in a very simple way. On timescales of  $10^5$ – $10^6$  years, water vapor is shuttled back and forth between the poles and equator spending enough time in each region for dust to mix with and settle on the ice, forming discrete layers. Such an explanation could account for hundreds of layers within the past 10 million years alone.

[6] Climate models seeking to understand the Martian climate and volatile systems over timescales for which orbital variability is important have typically been based upon a highly simplified representation of the atmospheric component [e.g., *Jakosky et al.*, 1993, 1995]. These models typically treat atmospheric transport as meridional diffusion. While such diffusivities may be “tuned” for the current climate (to fit water cycle observations, for example), extrapolation to other orbital states is problematic. It should also be noted that transport in the atmosphere is not necessarily well described by down-gradient diffusion (see discussion by *Haberle and Jakosky* [1990]). In this work, we take advantage of a validated, three-dimensional model of the Martian water cycle, described by *Richardson and Wilson* [2002a] and *Richardson et al.* [2002]. The advantage of such a model is that it provides some significant capability to self-consistently evolve a circulation and climate in response to varied orbital parameter forcing. While this self-consistent system may not properly represent a particular paleoclimate of Mars, it provides a significant improvement over previous, highly simplified models, and provides a strong basis for more refined future work. Since one can arguably incorporate an endless number of conditions and representations into a GCM, the interactions of these systems and conditions need to be carefully studied. The current model neglects several factors and processes which may ultimately be important in the climate cycle, such as regolith desorption of CO<sub>2</sub> under changing orbital conditions, the role of varied dust lifting as wind systems change, history-dependent surface water reservoirs, exchange of water with subsurface reservoirs, and the radiative feedback effects of increased volatiles in the atmosphere on surface ice. Ultimately, all of these effects will be incorporated, but nonetheless, the results presented here likely capture the broad first-order behavior of the volatile cycles due to their strong dependence on nonsubtle thermal forcing; this is why even simpler models have been credible.

[7] The following section outlines the model we are using for our calculations, its advantages and disadvantages. In section 2, we outline the primary components of our GCM. In section 3, we explain our philosophy and how we have designed our climate experiments. Section 4 describes results from our experiments for carbon dioxide, while sections 5 and 6 describe results for two sets of experiments for H<sub>2</sub>O. This is followed by an overall discussion of the

problem in section 7. Finally we summarize our findings in section 8.

## 2. Model

[8] This study uses the Geophysical Fluid Dynamics Laboratory (GFDL) Mars GCM for Martian climate simulations, which has been modified to incorporate physical parameters consistent with Martian processes and constants [Wilson and Hamilton, 1996]. Modifications include adjustments to the solar flux, surface albedo, gravity and topography. The model was also adapted to treat the condensation cycle of CO<sub>2</sub> and dust as a radiatively active, transported trace species. A detailed discussion of these changes is given by Wilson and Hamilton [1996], Wilson [1997], and Wilson and Richardson [2000]. The model resolution is 5° latitude by 6° longitude with 20 vertical levels. We have used the surface thermal inertia and albedo values of Palluconi and Kieffer [1981] and Pleskot and Miner [1981], respectively, but augmented them with polar albedo and thermal inertia data [Vasavada et al., 2000] to cover the entire global surface. The albedo and emissivity of dirty water ice are set to 0.38 and 1.0 for ice forming away from the north polar cap. The northern polar cap itself takes averaged values of albedo (0.37) and thermal inertia (598 Jm<sup>-2</sup>s<sup>-1/2</sup>K<sup>-1</sup>) from retrieved polar maps [Vasavada et al., 2000]. The CO<sub>2</sub> ice albedo and emissivity are prescribed at 0.6 and 0.8, respectively, as done by Hourdin et al. [1993], and are not tuned to fit Viking data. These values of CO<sub>2</sub> optical properties result in a closed seasonal cycle that generates seasonal ice caps and variations in surface pressure that compare well with observations. The composition of the polar caps mimics the present-day configuration, with a permanent water ice cap in the north, and a permanent CO<sub>2</sub> ice cap in the south. Radiative processes on Mars are a result of the time- and space-varying atmospheric dust and volatile fields, both of which differ substantially from Earth. The overwhelming majority of the atmospheric mass of Mars is comprised of radiatively active carbon dioxide, which is found as a trace species in the terrestrial atmosphere. Also, the presence of dust can substantially modify the Martian climate, while such effects are not found on Earth. Condensation of carbon dioxide takes place both at the surface and within the atmosphere whenever the grid box or surface temperature falls below the pressure-dependent condensation point. Within the atmosphere, CO<sub>2</sub> “snow” is assumed to instantaneously fall to the surface. Water ice clouds are treated using a “particle following” approach, whereby the cloud properties within an individual grid box are approximated by considering the response of a single particle to the average atmospheric variables within that grid box. Condensation occurs instantaneously at any time step in which the vapor pressure exceeds the saturation vapor pressure. In such a case, the saturation ratio is reset to unity, and the excess mass is converted to cloud ice within that grid box. Similarly, cloud ice is converted back to vapor when the saturation ratio drops below unity, until saturation is reached, or the cloud ice reservoir is exhausted. All water cloud ice particles are prescribed to be 2 μm in radius for sedimentation purposes, where the sedimentation rate is determined from the terminal velocity of the individual particle. Water can also exchange

directly with the surface. If the lowest atmospheric level is supersaturated, ice will form directly on the surface so as to reduce the lowest atmospheric level to the saturation point. Conversely, if ice is present on the surface beneath a subsaturated lowest atmospheric level, sufficient ice is sublimated from the surface to bring this level to saturation, or to exhaust the surface ice mass. While ice is present on the surface, the albedo is set to 0.38. The thermal inertia is not modified except in specific simulations, where stated. A more detailed outline of the incorporation of the water cycle into the model is given by Richardson and Wilson [2002a] and Richardson et al. [2002].

[9] Our various simulations, which shall be outlined in the following section, require the ability to change orbital parameters and surface ice location easily. The code has been designed such that a “startup” file is used to set these parameters without modifying the code itself. The simulations are initiated from a fully spun-up initial condition with present-day parameters. We then modify one or more parameters (obliquity, eccentricity, etc.) and let the model run toward a subsequently equilibrated seasonal cycle.

## 3. Philosophy and Design of Experiments

[10] The goal of this study is not to faithfully duplicate climate variability over orbital-change timescales, but rather to investigate basic mechanisms that control where, how and why volatiles exist for various orbital forcing. Our philosophy therefore was to eliminate several factors that would limit our ability to compare different simulations cleanly. Most notably, we have left out any regolith exchange of CO<sub>2</sub> or water vapor and the radiation effects of water vapor in the atmosphere. Furthermore, much can be learned about a system by its behavior out of equilibrium, and thus much of our attention is focused on the time within each simulation that the climate moves from a seasonal cycle equilibrated for one set of orbital parameters toward a subsequent seasonal equilibrium.

[11] In order to understand the nature of the volatile cycles under variations in orbital parameters, we have devised two broad sets of simulations (Table 1). The first involves long-term integration for fixed combinations of orbital parameters initialized with a GCM state that is fully thermally, dynamically and hydrologically spun-up for the contemporary set of orbital parameters. The second set is designed to provide further insight into processes and the uniqueness of the model solutions of the first set. Therefore they are integrated from a variety of initial states.

[12] Several simulations (s25, s35, s45, s60) for obliquities ranging from 25 to 60 degrees have been run. We do not describe simulations for low obliquity conditions (0°–25°), since at low obliquities, surface ice is stable only in the polar regions and does not make seasonal excursions to the tropics. Simulation s25 is our “standard” low obliquity simulation, and simulation s45 is treated as our baseline simulation for high obliquity conditions. Three runs (s45, s45p70, s45p160) look at the role of a varying argument of perihelion (the L<sub>s</sub> of perihelion) on the volatile cycles for conditions when perihelion is during late northern winter (L<sub>s</sub> = 251°), late northern spring (L<sub>s</sub> = 70°) and late northern summer (L<sub>s</sub> = 160°), respectively. On the basis of the results of Jakosky et al. [1995], which indicate little difference in

**Table 1.** List of Mars GCM Simulations Described in This Paper

Name	Obliquity	L <sub>s</sub>	Eccentricity	Notes
<i>Set 1</i>				
s25	25	251	0.093	Present-day conditions
s35	35	251	0.093	Most recent maximum obliquity excursion
s45	45	251	0.093	Standard “high obliquity” simulation
s60	60	251	0.093	Maximum simulated obliquity
s45p70	45	70	0.093	Perihelion occurs in late northern spring
s45p160	45	160	0.093	Perihelion occurs in late northern summer
s45e0	45	–	0.0	Circular orbit
s45e13	45	251	0.13	High eccentricity
<i>Set 2</i>				
s45si	45	251	0.093	Water ice cap moved from north to south pole. North pole albedo/thermal inertia set to average of surrounding ice-free regolith.
s45p70si	45	70	0.093	Water ice cap moved from north to south pole, perihelion occurs in late northern spring. North pole albedo/thermal inertia set to average of surrounding ice-free regolith.
s45wet	45	251	0.093	Entire surface covered with ice. Where ice exists, thermal inertia set to that of ice-filled (25%) regolith.
s45rev	25	251	0.093	Initialized from end of s45 sequence
s45dry	45	251	0.093	Removal of northern cap at end of s45. No change to polar albedo/thermal inertia.
s45thin	45	251	0.093	Placement of thin ice layer in north pole. No change to polar albedo/thermal inertia.
s35dry	35	251	0.093	Removal of northern cap at end of s35. No change to polar albedo/thermal inertia.
s45smooth	45	251	0.093	Averaging of tropical thermal inertia values to zonally constant value.

overall results between  $L_s = 160^\circ$  and  $L_s = 340^\circ$ , only one simulation has been performed in the near-equinox period. Eccentricity variations in Mars’ orbit occur on timescales of  $\sim 10^6$  years and chiefly determine the length of the seasons. Martian eccentricity ranges from nearly circular (0.0) to highly eccentric (0.13) [Ward and Rudy, 1992]. During low eccentricity, the seasons vary little in length. During periods of high eccentricity, however, the length of the seasons at aphelion is longer, while that at perihelion is shorter. It is the combination of both eccentricity and  $L_s$  of perihelion that determines the combination of a long or short and hot or cool season. Clearly this will have an influence on the size of the surface and atmospheric volatile inventories. Three runs (s45e0, s45, s45e13) consider the effect of low, medium and high eccentricity conditions.

[13] Set two consists of several “quasi-control” simulations. The first group (s45si, s45p70si, s25p70si), addresses several issues, including the stability of a northern polar cap, and the influence of the topographic dichotomy on volatile cycling. It is hypothesized that during previous epochs, the southern hemisphere may have had a substantial residual cap. Simulation s45si looks at a high obliquity state with the residual water ice cap moved from the north to south pole to address such a condition. Recent results [Richardson and Wilson, 2002b] seem to indicate that the topographic dichotomy on Mars drives the water cycle predominantly to the northern hemisphere. The other two simulations, s45p70si and s25p70si, can address this point if compared with s45 and s25, respectively. Because both the argument of perihelion and the location of the residual cap are reversed in each pair, this is equivalent to an experiment in which the topography of the planet is flipped north–south. This experiment isolates the effect of the global mean topographic dichotomy on the volatile cycles and thereby

specifically addresses the ideas raised by Richardson and Wilson [2002b]. In a second group (s45si, s45thin, s45dry, s35dry), we have adjusted the thickness and/or position of the north polar cap to determine its stability under high obliquity. Essentially, we are asking the question “Is the presence of at least a small north polar cap required at high obliquity?” In another run, (s45wet), we seek to understand the effect that surface ice has on climate feedback, namely the ice-albedo-thermal inertia feedback. With this experiment, we aim to determine whether climate can recover from a so-called “Snowball Mars” state based purely on orbital variations, or whether a separate trigger is required to return to more clement conditions. In simulation s45rev, we look at isolating hystereses conditions—perhaps those found in every orbital cycle. Namely, what is the overall effect of boosting obliquity to  $45^\circ$  for a period, then returning to present-day ( $25^\circ$ ) conditions? Do fields such as the surface ice abundance return to their  $25^\circ$  obliquity amounts, or is there a secular change over the course of each cycle? Lastly, as we shall note, thermal inertia plays a critical role in determining the location of surface ice at high obliquity. The simulation s45smooth looks at the extent of this effect by adjusting low-latitude thermal inertia to “smooth out” the ice deposition mechanism. We refer the reader to Table 1 for more detailed comments regarding the setup of each simulation.

#### 4. Variations in the CO<sub>2</sub> Cycle

[14] The present-day Martian pressure cycle (Figure 1, where we use total atmospheric mass as a proxy for “average” Martian pressure) oscillates over the course of the year as a result of the varying thermal conditions on Mars, and the consequent condensation/sublimation cycle of

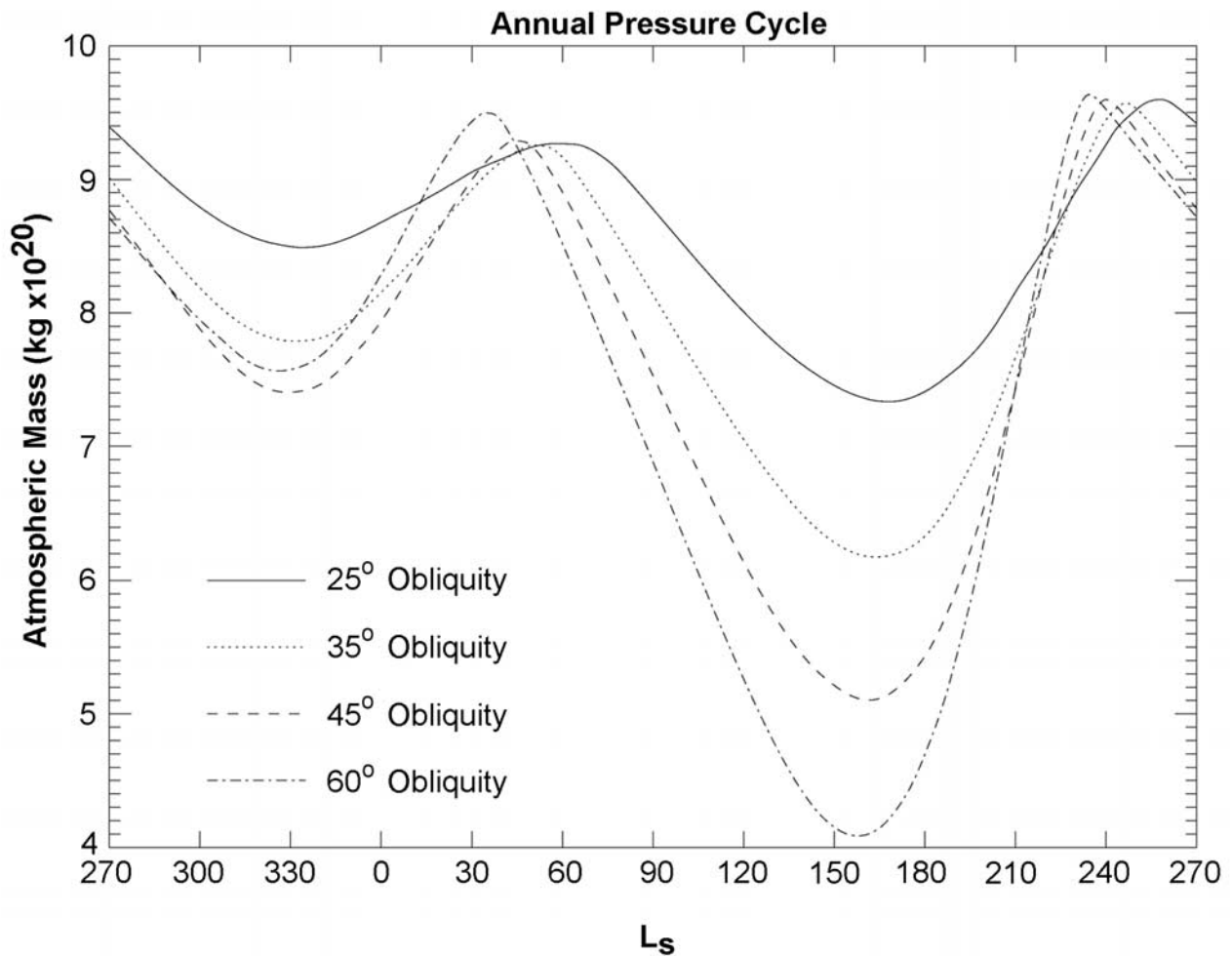


**Figure 1.** Globally integrated atmospheric mass over a single Martian year for four different obliquities. Dips in each curve correspond with the northern and southern hemisphere winter season (from left to right).

carbon dioxide. Such behavior was suggested by *Leighton and Murray* [1966] and has been fully recorded over several Martian years [*Hess et al.*, 1979, 1980; *Tillman*, 1988] and modeled [*Briggs*, 1974; *Pollack et al.*, 1976, 1981, 1990, 1993]. Figure 1 illustrates the atmospheric mass cycle over several obliquity states. At each state, the same general behavior is seen. Every year sees two dramatic dips in atmospheric mass, the result of atmospheric deflation in the winter hemisphere. The southern winter “dip” is greater than that of the northern winter because Mars’ position near aphelion results in a longer southern winter. Temperatures remain at the CO<sub>2</sub> frost point for a greater time, and more of the atmosphere is lost to the surface. Under present conditions, there is a variation in atmospheric mass of ~25% over the course of a year. Total deflation increases with increased obliquity as a greater fraction of the winter hemisphere is covered in the cold darkness. At 35°, the cycle varies by 36%; at 45°, it is 47%, and at 60°, the value rises to 58% or, in other words, the global atmospheric pressure is reduced by nearly two-thirds during southern winter at 60° obliquity. Studies of the magnitude of atmospheric deflation have been performed by *François et al.* [1990] and more recently by *Haberle et al.* [2003].

[15] We can understand the complete CO<sub>2</sub> cycle as a combination of the three spatially and temporally varying components detailed by *Hourdin et al.* [1993], the most evident component being the condensation/sublimation cycle of CO<sub>2</sub>, with surface orography and local dynamics playing important, but largely secondary roles. Clearly, the northern lowlands will have a higher surface pressure than their southern highland counterpart, at least in an annually averaged sense, due to their lower elevation. This is seen in the overall higher surface pressures in the northern hemisphere within each panel of Figure 2. Sublimation explains the presence of high pressure over the late-spring seasonal caps, as the influx of new CO<sub>2</sub> from the seasonal cap inflates the surface pressure. A low-pressure signature ought to be observed, then, over the condensing, autumn/winter seasonal cap for the opposite reason; however, that signature is masked by the greater influence of the global dynamics. Specifically, pressure gradients across the tropics and midlatitudes develop as a result of the thermally driven Hadley circulation. High pressure develops in the winter hemisphere beneath the descending branch and is associated with surface-level divergence and vice versa in the summer hemisphere. Thus, although CO<sub>2</sub> is lost to the seasonal cap,

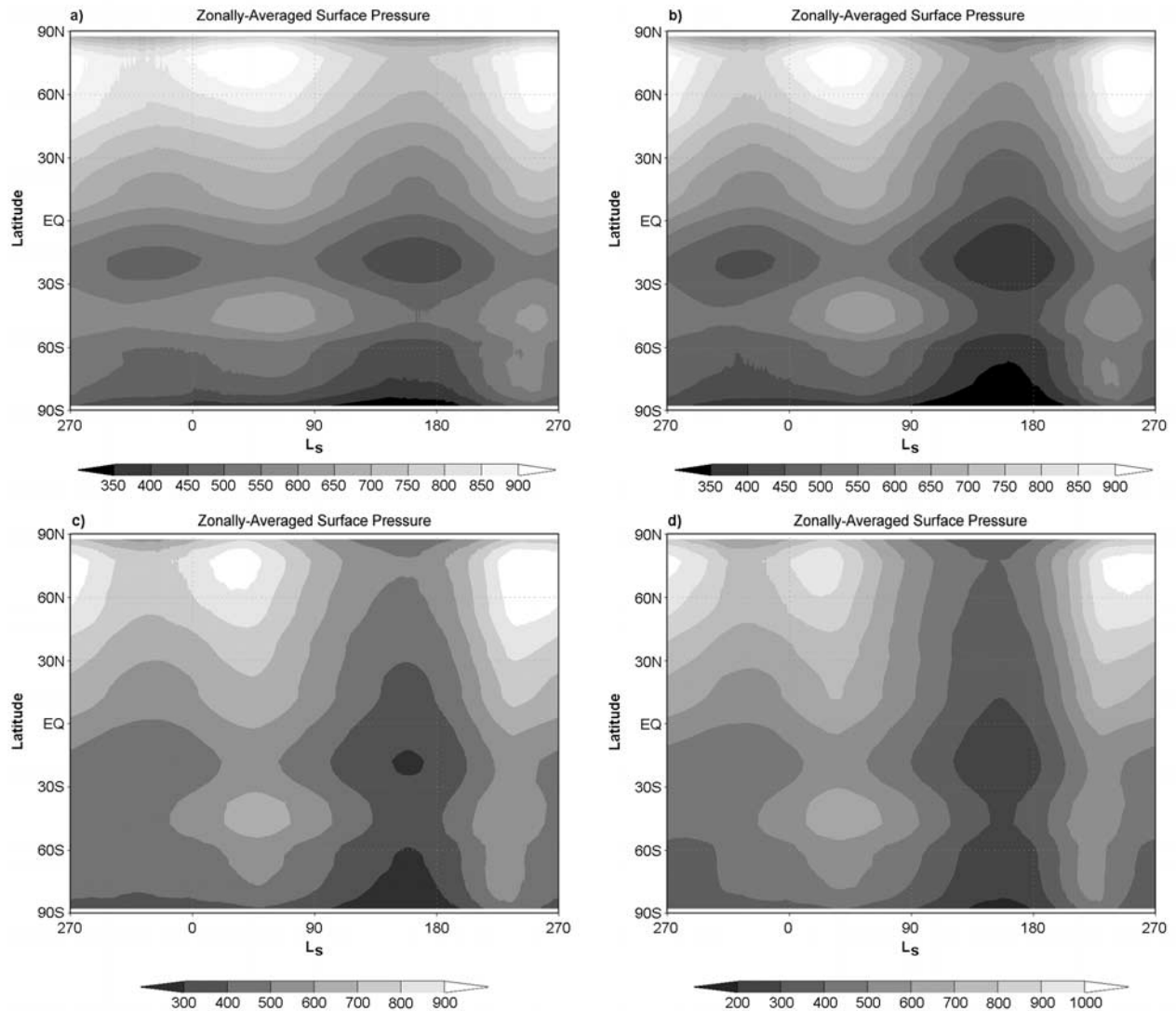


**Figure 2.** Zonally averaged surface pressure in Pa for a full Martian year at (a) 25° obliquity, (b) 35° obliquity, (c) 45° obliquity and (d) 60° obliquity. Two maxima are evident simultaneously in each hemisphere, one due to sublimation of the seasonal CO<sub>2</sub> cap and the other dynamically influenced by the descending branch of the Hadley cell.

the loss is partially offset by the increased pressure of the downwelling atmosphere. Such behavior is noted by *Hourdin et al.* [1993].

## 5. Water Cycle

[16] The design of the water cycle experiments was described in section 3. In this section, we examine the evolution of the modeled water cycle, with specific emphasis on the distribution of surface ice, the abundances of atmospheric water vapor and cloud ice, and the processes contributing to equilibration of the modeled cycles. This latter aspect of the study is crucial for determining whether various surface ice reservoirs are stable, and for understanding the rates of exchange between the major water reservoirs. Analysis of the water cycle budgets and stability will employ a modified version of the diagnostic approach described by *Richardson and Wilson* [2002a]. Specifically, we include a budget for tropical (30°S–30°N) surface water

ice in order to track shifts in water between the poles and the tropics (this was not necessary for consideration of the current Martian water cycle). These budgetary elements are shown in Figure 3.

### 5.1. Effect of Obliquity

[17] Obliquity has a dramatic effect on the annually averaged and annual peak radiative heating of the polar regions. Simplified models [*Jakosky*, 1983a, 1983b; *Jakosky et al.*, 1993, 1995] and full three-dimensional climate models [*Richardson and Wilson*, 2002a] agree that the primary determinant of the atmospheric humidity is the residual water ice cap temperature. Thus large changes in cap surface temperature resulting from large changes in summer insolation should drive dramatic differences in equilibrium vapor abundances (see also *Jakosky et al.* [1993, 1995]). Thus we initially concentrate on changes in the modeled water cycle resulting only from changes in obliquity. As in section 4, we have used four simulations

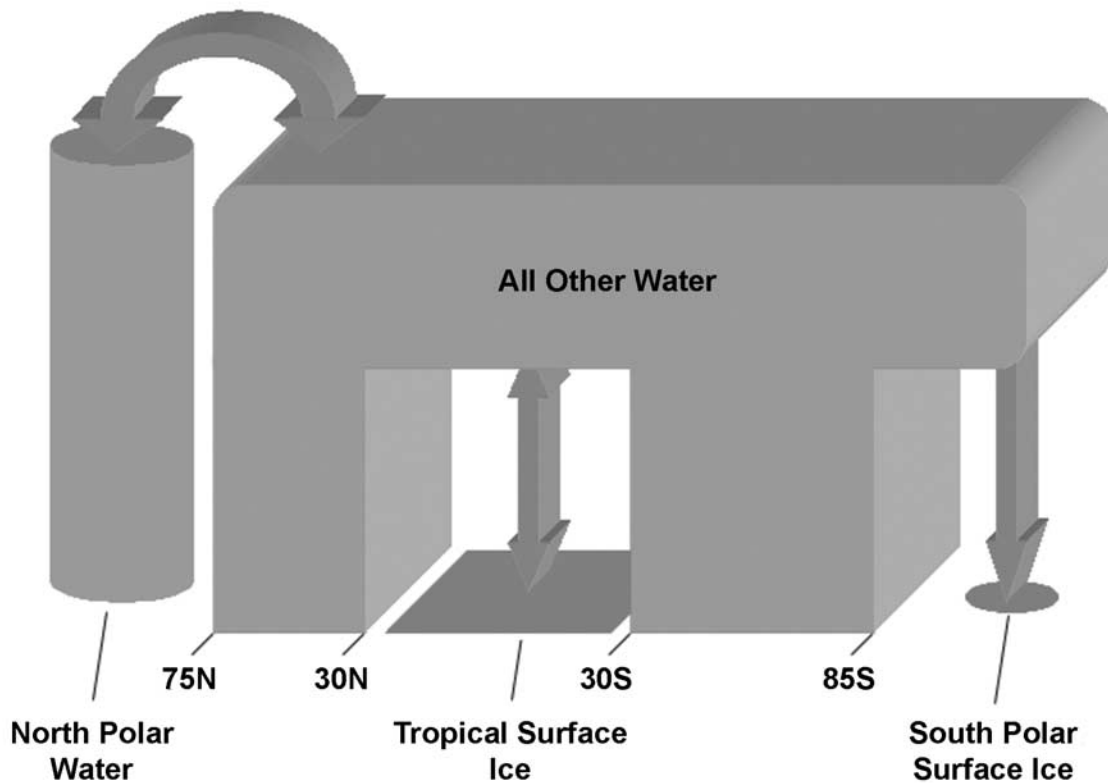


**Figure 3.** Cartoon illustrating the four water reservoirs we consider in this work. Water is lost from the north polar cap into the atmosphere (“North Polar Water”), where it is transported in different amounts to the midlatitudes, tropics or south polar cap. At low obliquity ( $<25^\circ$ ), water vapor returns every autumn/winter to the polar cap, indicated by the two-way arrows between the North Polar Water and “All Other Water” reservoirs. At moderate obliquity ( $35^\circ$ ), water vapor is preferentially deposited in the cooler midlatitudes (part of the “All Other Water” reservoir), while at high obliquity ( $>45^\circ$ ), it is deposited in the tropics. The slow, one-way sink of water vapor to the south polar cold trap occurs regardless of obliquity.

(s25, s35, s45, s60) with obliquities stepping from  $25^\circ$  to  $35^\circ$ ,  $45^\circ$ , and  $60^\circ$ . As an initial condition, we have established a water ice cap in the northernmost two grid points ( $82.5^\circ\text{N}$ – $87.5^\circ\text{N}$ ) and have set a permanent CO<sub>2</sub> ice cap “cold trap” at the southernmost ( $87.5^\circ\text{S}$ ) grid point, with no initial surface water ice anywhere else on the planet.

[18] The s25 run is the low-obliquity control simulation. Figure 4 shows the evolution of zonal-average surface ice (Figure 4a), atmospheric vapor (Figure 4b) and cloud ice (Figure 4c), along with the diurnal- and zonal-average annual cycle in surface temperature (Figure 4d). Following the drift toward equilibrium, the vapor amounts peak in northern summer just between  $70$ – $80$   $\mu\text{m}$ . The vapor distribution shows a monotonic latitudinal decrease in northern summer, and a double peaked distribution in southern summer, illustrating the relative importance of the Hadley circulation [Richardson and Wilson, 2002a]. Cloud ice accounts for a modest fraction of the atmospheric water budget, with peak nonpolar cloud ice developing as part of the tropical cloud belt [Richardson et al., 2002]. Polar hood clouds are evident also. These control simulations compare well with the “best fit” simulations described by Richardson et al. [2002], and hence generally with the

Mars Atmospheric Water Detector and Thermal Emission Spectrometer observations.

[19] The effect of increasing obliquity to  $35^\circ$  can be gauged by comparing Figures 4 and 5. As the s35 simulation trends to equilibrium, the northern polar atmosphere is seen to hold over  $1200$   $\mu\text{m}$  (Figure 5b), representing an order of magnitude increase over the  $25^\circ$  case. This increase is directly caused by higher cap temperatures, and through the influence of cap temperatures on the temperature (and hence holding capacity) of the overlying air. For this same reason, namely that the southern summer is warmer than the northern summer in this configuration, the southern hemisphere vapor peak in s35 is higher than that of the north, with column amounts over  $2000$   $\mu\text{m}$ . Despite the larger meridional vapor gradient during southern summer versus northern summer, examination of model output (not shown) shows that there is still a net, annual transport of water from north to south. This must result from either the shorter period of southern summer or differences in transport and/or the vapor gradient. The latter is unlikely, as it has been shown [Richardson and Wilson, 2002b] that the south-to-north transport is more effective. Cloud water ice dramatically increases, with a significant tropical cloud belt developing year-round. Cloud amounts exceed  $1200$   $\mu\text{m}$

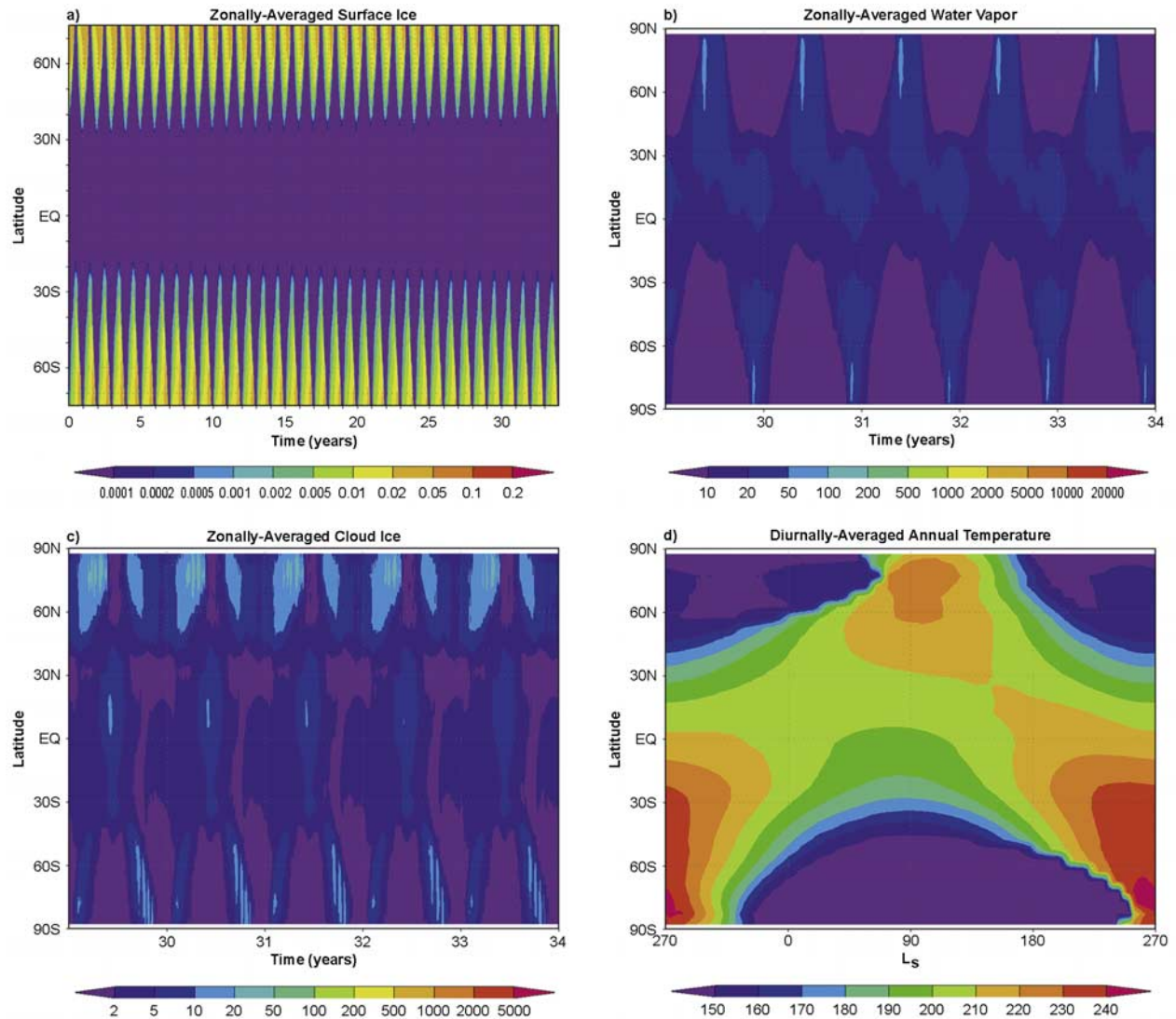


**Figure 4.** (a) Zonally averaged surface ice over 34 Martian years at 25° obliquity. Colors indicate ice thickness in cm. At low obliquity, seasonal caps do not extend to the tropics. Latitudes poleward of 75° in this and subsequent surface ice maps have been removed to preserve dynamic range in midlatitudes and tropics, and enhance figure clarity. (b) Zonally averaged atmospheric water vapor abundance over the last 5 years of the simulation (model years 29–34) measured in pμm. (c) Zonally averaged water ice cloud abundance over the last 5 years of the simulation (model years 29–34), measured in pμm. (d) Diurnally and zonally averaged surface temperature (in K) for one Martian year.

(Figure 5c) during southern summer. Thus the model predicts that over half the water in the atmosphere away from the poles is in the form of cloud ice. As a result of the increased atmospheric water abundance, the extent of the seasonal cap grows significantly. After several seasons, the equatorward extent of each seasonal cap overlaps (Figure 5a), which suggests that surface ice will exist at all latitudes across the planet. This is not to suggest that surface ice is ubiquitous, but merely that thermal conditions at the surface are conducive to ice formation everywhere at some point during the year. Perennial ice forms in this simulation in the region between 55°N and 75°N, as that band has become dynamically and thermodynamically favored. It should also be noted that in this simulation, the ice does not form a continuous annulus around the northern pole, but instead

develops distinct ice sheets as shown in Figure 6. At 35° obliquity, the seasonal water ice cap covers approximately one-half of the Martian surface at its maximum. The red and orange regions found in the high, northern midlatitudes in Figure 5 and which indicate the greatest zonally averaged amount of ice, come about as a result of these few distinct regions of very thick ice in Figure 6, while the remainder of the surface is covered by, at most, a few millimeters. The location of these regions depends strongly on the thermal inertia of the underlying regolith (see section 6.1). As such, the fact that the model neglects subsurface diffusion and freezing of water and consequent modification of thermal inertia, means the model may not properly represent the uniformity of surface ice formation within the latitudinal band of stability.

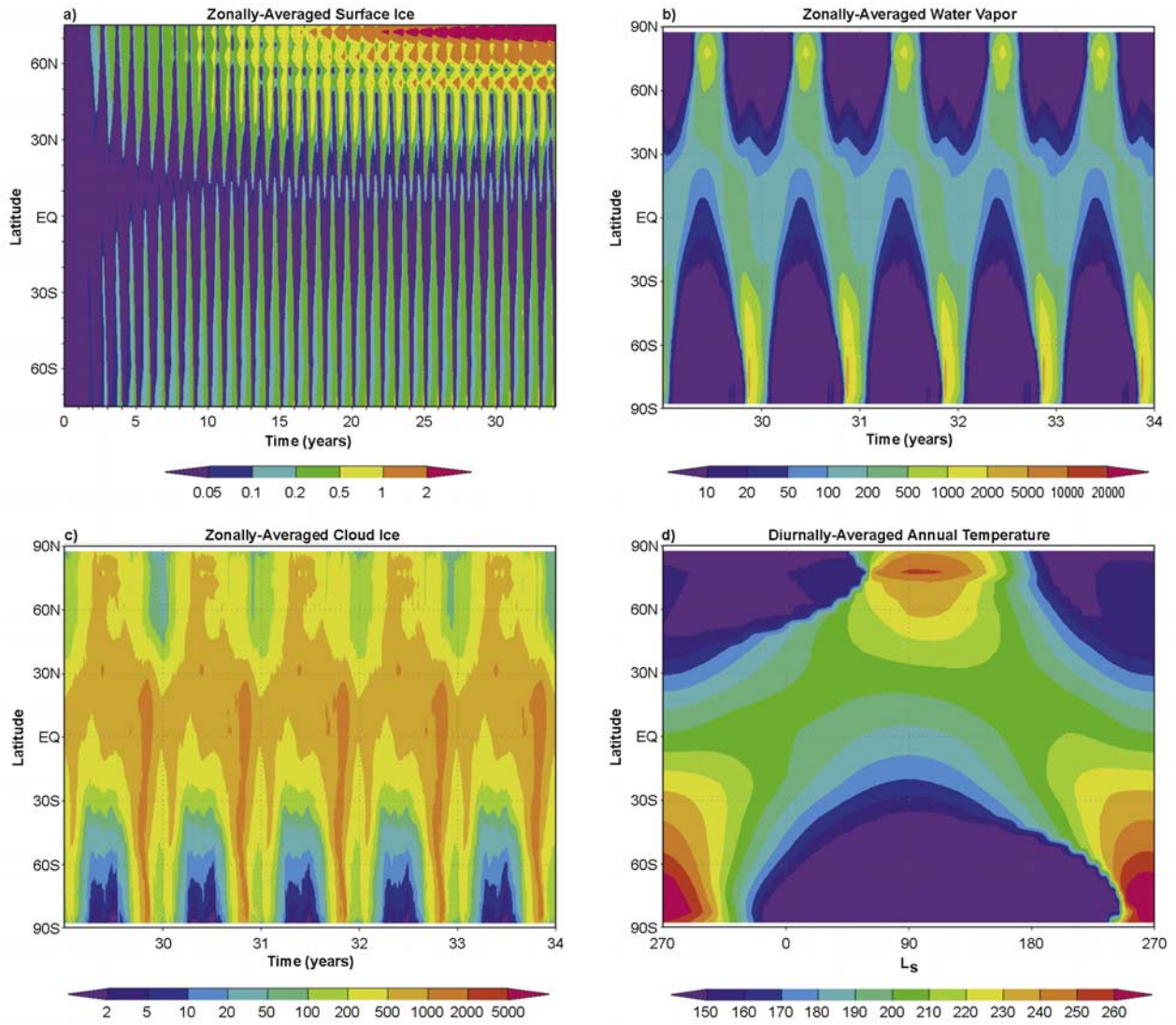


**Figure 5.** Same as Figure 4, but at  $35^\circ$  obliquity. Note the greatest thickness of surface ice occurs in a ring within the midlatitudes ( $55^\circ$ – $75^\circ$ N), rather than at the poles.

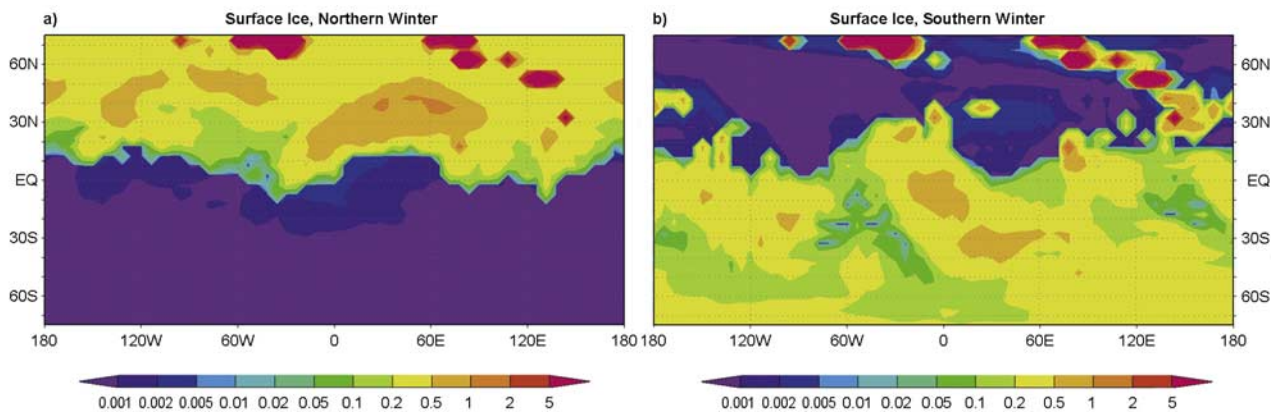


**Figure 6.** (a) Maximum extent of seasonal water ice cap during northern hemisphere winter at  $35^\circ$  obliquity. (b) Maximum extent of seasonal water ice cap during southern hemisphere winter. Colors indicate ice thickness in cm.

[20] The s45 simulation (Figure 7) extends trends evident in the s35 case. Water vapor now peaks at over 3600  $\mu\text{m}$  in the northern polar region (Figure 7b). Southern polar water has a similar maximum. The evolution of the latitudinal profile of vapor now clearly follows the pattern of ground temperature. The tropical vapor abundances peak at just below 400  $\mu\text{m}$ . This is only a 10–20  $\mu\text{m}$  higher than at 35°, and similar to that found at 60° obliquity (see below). By 35° obliquity, the model atmosphere has come close to the nighttime holding capacity for water vapor, with additional polar vapor generated as obliquity increases being unable to further increase tropical vapor amounts. Cloud amount peaks in southern summer at over 2500  $\mu\text{m}$  (Figure 7c). As seen in Figure 7a, surface ice remains stable at the low latitudes year-round. Again, this is not at all longitudes, rather at select points, but the same caveat mentioned above should be borne in mind. Nonetheless, these points remain frost-covered throughout the year. The maximum extent of the seasonal caps is found in Figure 8. At the conclusion of our simulation (about 34 Martian years), the extent of this “tropical band” of ice appears to have nearly, but not completely, stabilized. With each passing season, the poleward edges of this band creep slightly poleward. This slight variation is worth following, as it suggests the development of a perennial frost cover across Mars, were the band continue to creep poleward. We shall examine the possibility of this phenomenon in a later section.

[21] The 60° obliquity case represents the extrema of our studies (Figure 9). Northern polar vapor peaks at over 10,000  $\mu\text{m}$  (Figure 9b), with southern polar water peaking at just below half this value. Peak tropical vapor remains limited to  $\sim$ 400  $\mu\text{m}$ . Clouds are now ubiquitous, at levels exceeding 4000  $\mu\text{m}$  in the southern summer tropics (Figure 9c). In this case, there is nearly full tropical coverage of surface ice, at all longitudes, and at all seasons (Figure 10). As with the s45 simulation, the “tropical surface ice belt” continues to grow in size, and we shall see when/where this will equilibrate in a later section. These figures also suggest that surface ice is no longer stable in the mid and high latitudes.

[22] By comparing the annual temperature cycles (Figures 4d, 5d, 7d, and 9d), it is apparent that at higher obliquity, lower latitudes become thermodynamically favored. At all obliquities, the temperature range at the equator is quite modest, and the extremes decrease with increasing obliquity. Conversely, at the poles, the temperature range is quite large (up to 150K at 60° obliquity, Figure 9d), and the maximum extreme increases with increasing obliquity (the minimum extreme remains at the CO<sub>2</sub> frost point). Surface ice will be preferentially deposited at the location with the lowest “average” annual temperature.

[23] The exchange processes occurring within the four model simulations are better illustrated in Figure 11. These budget elements correspond to those illustrated in Figure 3. As it is the northern polar cap providing the water for this system, we are at liberty to choose an arbitrary thickness for the northern cap, so long as it is thicker than the extent of the annual thermal wave. The model does not care if the polar cap is one meter thick or 5 kilometers thick, as only the uppermost meter or so is interacting with the atmosphere. This has its advantages, as we need not concern

ourselves with estimating the thickness of the northern cap, however in Figure 11, the arbitrary size of the north polar reservoir means the values of northern cap mass are shifted down by some arbitrary amount to facilitate understanding of the plot. It is not necessary to know the absolute thickness of the northern cap, as long as we can measure its annual change. The s25 case presents a cycle very similar to that shown by *Richardson and Wilson* [2002a]. The s25 case (Figure 11a) reaches an approximate equilibrium in the 34 years shown with the northern polar budget becoming repeatable after the first few years. The net change is due to the southern polar cap drawing down water vapor from the atmosphere. Small amounts of water are found seasonally in the tropical surface ice budget, resulting from the equatorward edge of the southern seasonal ice cap. The initial rise in nonpolar water is due to the initiation of this simulation from an early s35 case, and not from a dry case as was done for the other simulations. Our intention here was to over-saturate the initial s25 system, and bias the 25° case to wetter amounts, thereby presenting a conservative estimate of the effect of obliquity on the water cycle through comparison with the higher obliquity simulations. Despite being much drier than any of the higher obliquity cases, the net flux in the s25 case is of water from the low-latitudes to the high-latitudes, tending to return to the state observed and described for the current climate.

[24] The s35 budgets (Figure 11b) show a more dramatic trend in northern polar water. In just 30 years, the cap loses over  $6 \times 10^{14}$  kg of water, corresponding to a loss of about 60 cm of water from the cap (note that this is not a steady state loss rate, being significantly higher than the steady state value). This water is transferred to each of the three other budgetary elements. The actual transport pathway is a little more complex: in northern summer, water is moved from the northern polar cap, rapidly through the atmosphere, to the midlatitudes and tropics (which corresponds to the northernmost extension of the “southern” seasonal ice cap at this time). In northern autumn, winter, and spring, there is a much more modest return flow of water to the northern polar cap, as well as toward the southern residual cap. Due to the lower vapor gradient during return flow, vapor builds in the tropics and midlatitudes, and remains there until the following northern summer. The combination of the midlatitude atmosphere becoming saturated, the moderate pole-to-equator flow, and the relatively cooler temperatures causes this region to develop surface ice. A close look at the individual budgets highlights this point. The midlatitude water reservoir is steadily increasing at the expense of the depleting north polar reservoir. At 35°, the tropical reservoir has equilibrated at some nominal value. Were the simulation to run indefinitely, we would likely see the buildup of thick deposits of ice in the midlatitudes (a steadily rising midlatitude water line) until the north polar ice was fully depleted (a steadily decreasing north polar ice line).

[25] At 45° and 60° obliquity, the loss rate of northern polar water is enhanced. In 30 years, the northern polar cap loses 6 m of ice in s45, and almost 32 m in s60. More importantly, unlike in the s25 case, there is no indication that the loss rate will eventually reach a steady state allowing the residual northern polar water ice cap to be

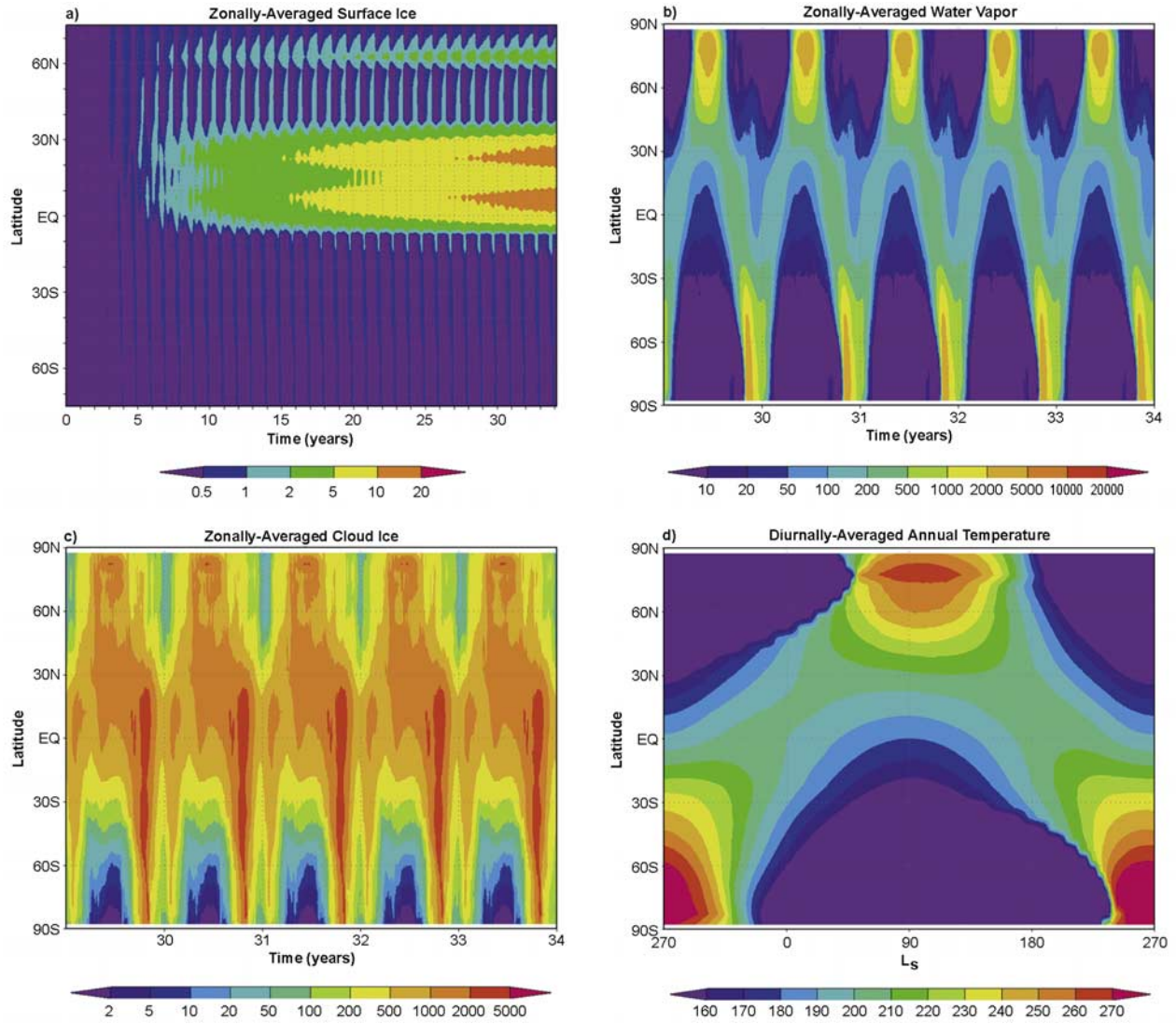


**Figure 7.** Same as Figure 4, but at 45° obliquity. Now, surface ice is most predominant in a band within the tropics.

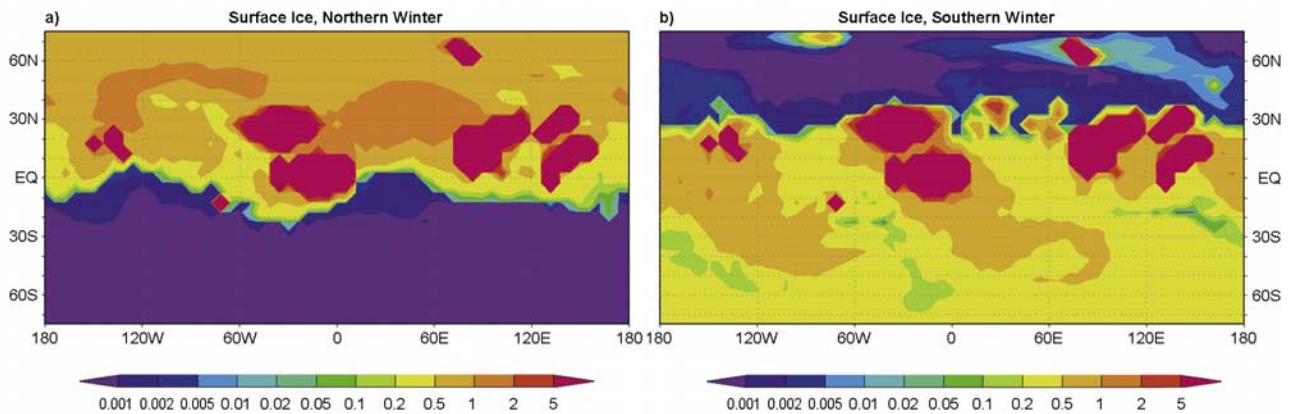


**Figure 8.** Same as Figure 6, but at 45° obliquity. Large pink regions are locations of thickest surface ice, and correlate to surfaces of high thermal inertia and/or high topography. These regions remain ice-covered year-round.

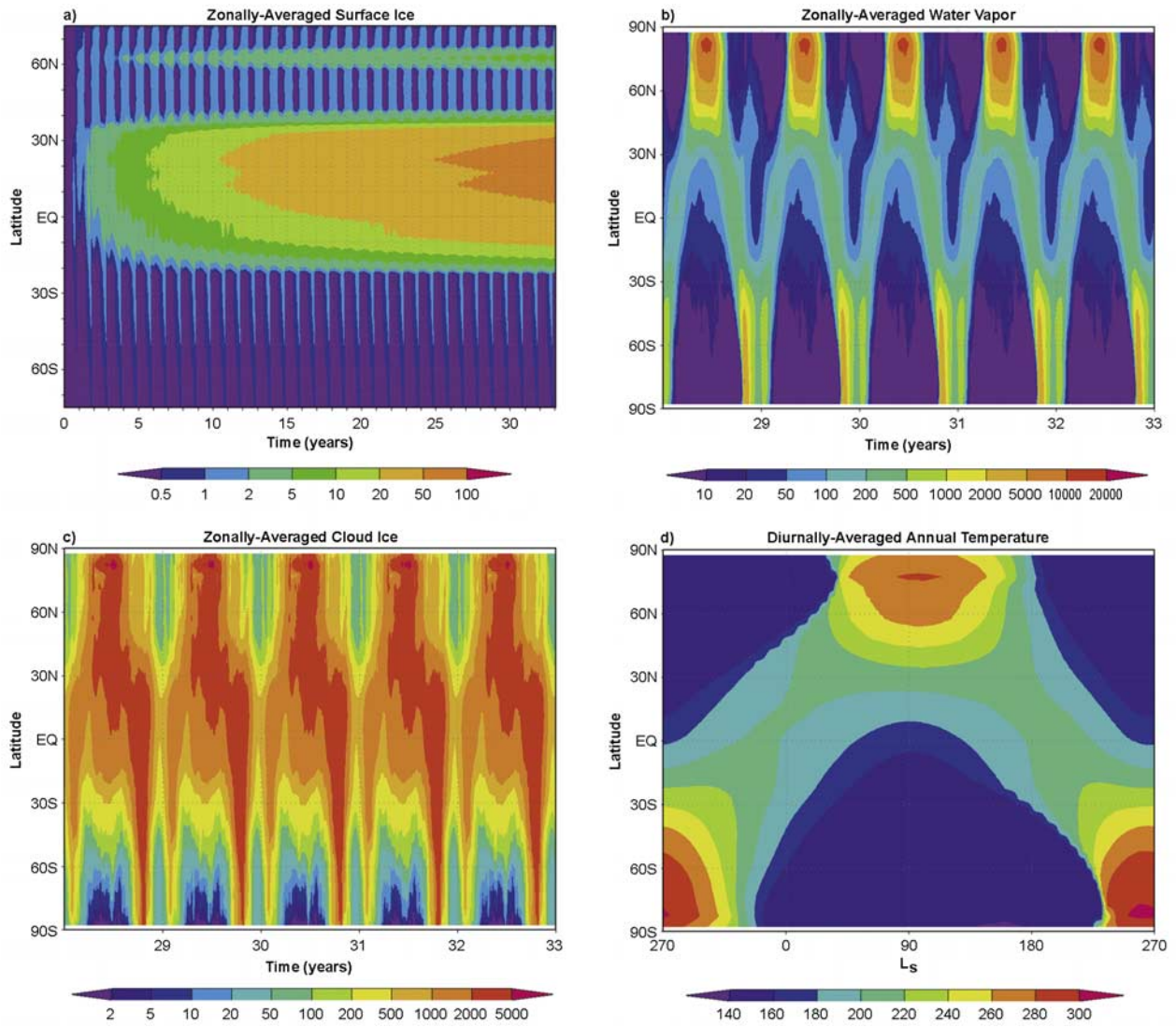


Figure 9. Same as Figure 4, but at 60° obliquity.

stable. More broadly, we showed above that in the s35 case, the northern polar water and midlatitude reservoir are the budgetary elements that change in order to move toward equilibrium. For s45 and s60, the midlatitude water budget

rapidly (~7 years for s45 and ~3 years for s60) comes to an interannually repeatable state. From that point on, s45 and s60 primarily involve a direct and linearly trending exchange between northern polar water and tropical surface

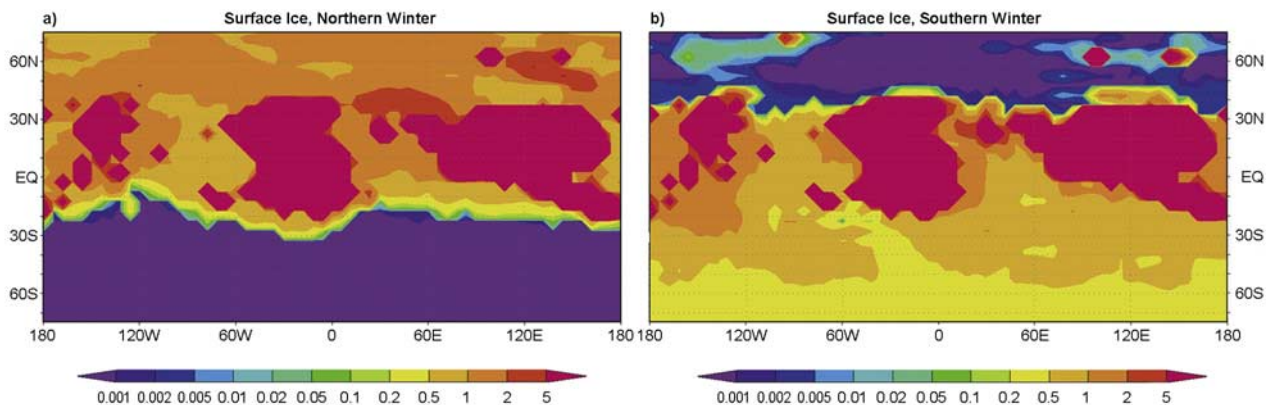
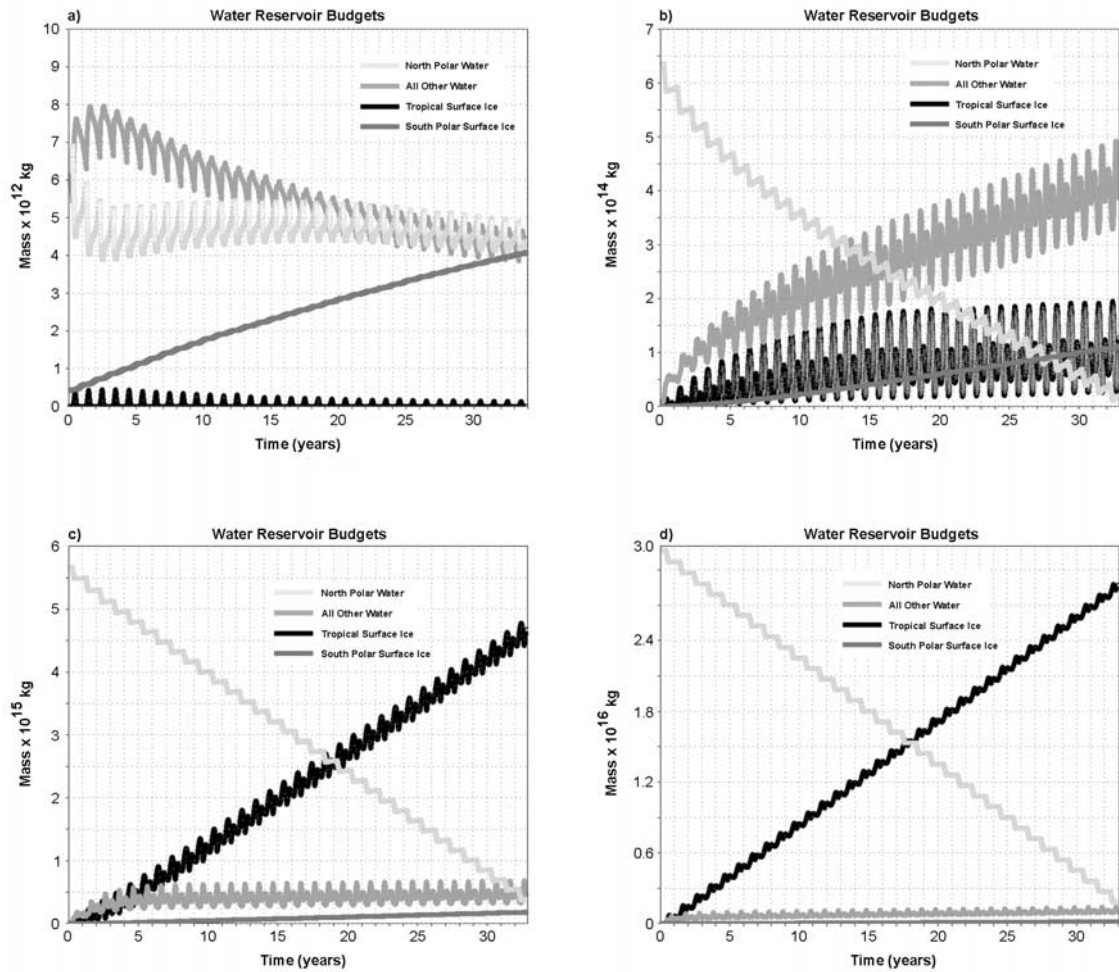


Figure 10. Same as Figure 6, but at 60° obliquity.



**Figure 11.** (a) Water budgets for the four reservoirs outlined in Figure 3, determined at  $25^\circ$  obliquity. Under low obliquity conditions, water is shuttled back and forth between the north pole and midlatitude reservoirs, with slow leakage to the south polar cap. Initial abundance of north polar ice was arbitrarily chosen at a value far above the other reservoirs (see text for explanation). For clarity, north polar curve has been shifted to approximately same values as other reservoirs, and so ordinate labels do not correspond to actual north polar reservoir mass. (b) Same as (a), but at  $35^\circ$  obliquity. Here, midlatitude ice increases with time at the expense of the north polar cap. Tropical ice reaches equilibrium value corresponding with a saturated overlying atmosphere. (c) Same as (a), but at  $45^\circ$  obliquity. Here, tropics are preferred location for surface ice. Warmer midlatitudes quickly reach an equilibrated seasonal cycle. (d) Same as (a), but at  $60^\circ$  obliquity.

ice. This limiting of midlatitude water is primarily due to saturation of the nighttime atmosphere. Once saturated, this budget can no longer buffer the water cycle, and simply acts as a conduit for transfer between the pole and tropics. Unlike for s35, however, the “coolest” location on the planet is in the tropics, and so ice is deposited here, rather than in the midlatitudes. We can imagine the atmospheric reservoir as a box representing its holding capacity (Figure 3) and which is filled completely at night. During daytime, the size of the box “grows” as the temperature rises. Water transported from the north polar reservoir can trickle into the box, such that the daytime vapor pressure exceeds the nighttime saturation pressure. As the temperature falls in the evening, this excess water gets “squeezed” out of the box, and deposited elsewhere. Since the coolest temperatures fall on the equatorward

edge of the box, this excess water will be deposited as ice at this cold trap location.

[26] The saturation of the nighttime atmosphere at both low and high obliquity is illustrated in Figure 12. This example comes from northern summer. At low obliquity (Figure 12a), much of the midlatitudes and tropics are sub-saturated, especially during daytime when the atmosphere experiences peak temperatures and therefore peak holding capacity. At high obliquity (Figure 12b), the change is quite drastic. During this season, the atmosphere is fully saturated at all locations except for the northern high latitudes during the daytime. During the daytime, the vapor amount rises, but not as quickly as the holding capacity yielding an atmosphere that is marginally sub-saturated (in a column-integrated sense). Therefore water vapor mass cannot increase much beyond the levels that develop in the

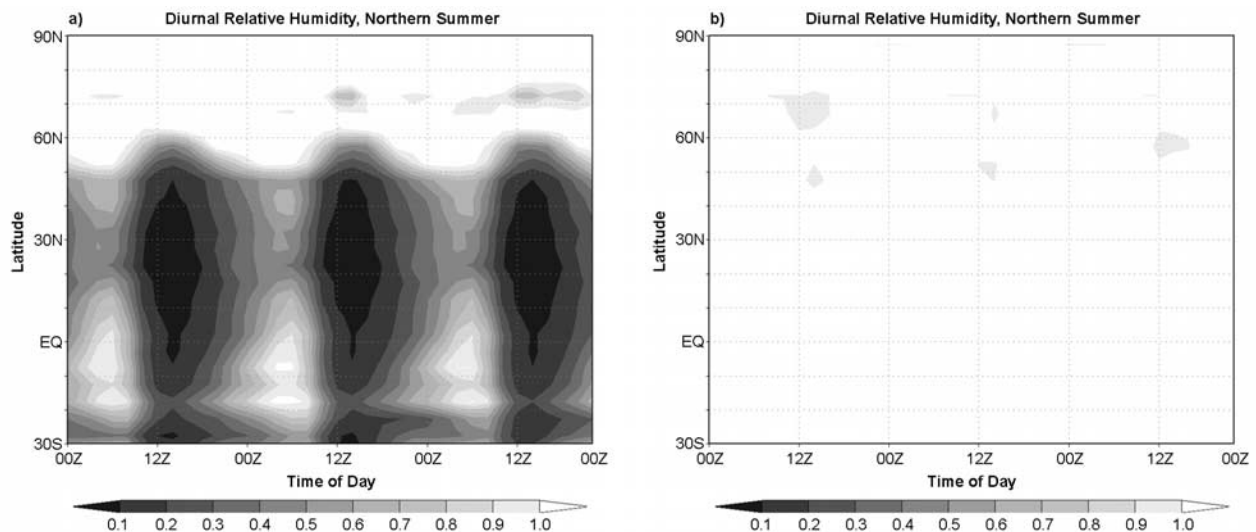


**Figure 12.** (a) Column-integrated relative humidity over three northern summer days at  $0^\circ$  longitude, and at  $25^\circ$  obliquity. Midlatitudes and tropics are highly sub-saturated during full diurnal cycle. (b) Same as (a), but at  $45^\circ$  obliquity. Now, entire atmosphere is saturated, except briefly in midlatitudes during daytime.

s35 simulation, and hence the nontropical/nonpolar water budget loses its buffering capability.

## 5.2. Effect of Eccentricity

[27] One effect of eccentricity is to change the distance from the planet to the Sun at aphelion, and thus as eccentricity increases, to make the aphelion winter much longer and colder than the complementary season one half-orbit later. For the present argument of perihelion, increasing the eccentricity would make the northern (southern) hemisphere winters (summers) shorter and warmer, and the northern (southern) hemisphere summers (winters) longer and cooler. For increased eccentricity (s45e13), the northern water ice cap is exposed to the Sun during a longer, cooler summer. The effect of high eccentricity is thus to decrease the polar cap heating rate due to reduced insolation, and hence to reduce northern polar cap surface temperatures. Due to the nonlinearity of the saturation vapor pressure with temperature, the total amount of water sublimated from the northern polar cap is reduced compared to that lost at present eccentricity. As a consequence, the amount of surface water ice found in the nonpolar regions is correspondingly reduced (Figure 13c).

[28] The shift of the zonally averaged surface ice deposits to the north at high eccentricity is also readily attributed to the modified polar cap heating rates (both north and south). During the southern hemisphere spring/summer, the increased heating rate will quickly sublime the south seasonal ice cap and transport it northward. Conversely, the reduced polar heating rate insures that the northern cap is less able to sublime and transport water than under current conditions. As a result, the balance between south-to-north and north-to-south water transport shifts northward (Figure 13c).

[29] The other extreme would be an orbit with zero eccentricity (s45e0). Relative to current conditions, northern polar cap temperatures are higher, leading to greater sublimation of water and more water being available outside the

northern polar regions. Thus the tropical ground ice is thicker for the zero eccentricity simulation (Figure 13a). The hemispheric transport bias described above is largely squelched, since both poles experience the same heating rates in their respective summers, hence the ground ice is located nearly symmetrically between the two hemispheres. A minor shift toward the northern hemisphere exists due to the biasing of circulation by the global topographic slope [Richardson and Wilson, 2002b].

## 5.3. Effect of Argument of Perihelion

[30] Tightly coupled to eccentricity is the orbital position of perihelion, which determines the season of closest approach to the Sun, and indirectly the relative length and intensity of the two summers. Presently, perihelion occurs at  $L_s = 251^\circ$ , which is late northern autumn/early winter. This minimizes the loss of water from the northern cap due to the relatively low heating rates resulting from being at aphelion during summer. During the opposite scenario, when perihelion occurs during northern spring/summer (s45p70), water loss is enhanced due to the closer proximity of Mars to the Sun. This is evidenced by the relative abundance of surface ice for these two cases in Figures 14a and 14c.

[31] The location of surface ice follows the logic outlined in section 5.2. The warmer summer hemisphere has a greater ability to sublime and transport water from the cap to the rest of the planet, pushing the position of the tropical ice deposits toward the cooler hemisphere. An intuitive way of seeing this is to note that the hemisphere where the ice is resident is, annually, the “cooler” of the two hemispheres. Whereas winter temperatures in both hemispheres are pegged at the CO<sub>2</sub> condensation point, the summer at perihelion will be warmer than the summer at aphelion, driving the ice toward the aphelion summer hemisphere. For s45, this is the northern hemisphere, while for s45p70, this is in the south.

[32] A final simulation, s45p160, was performed with perihelion occurring close to equinox, and as we should

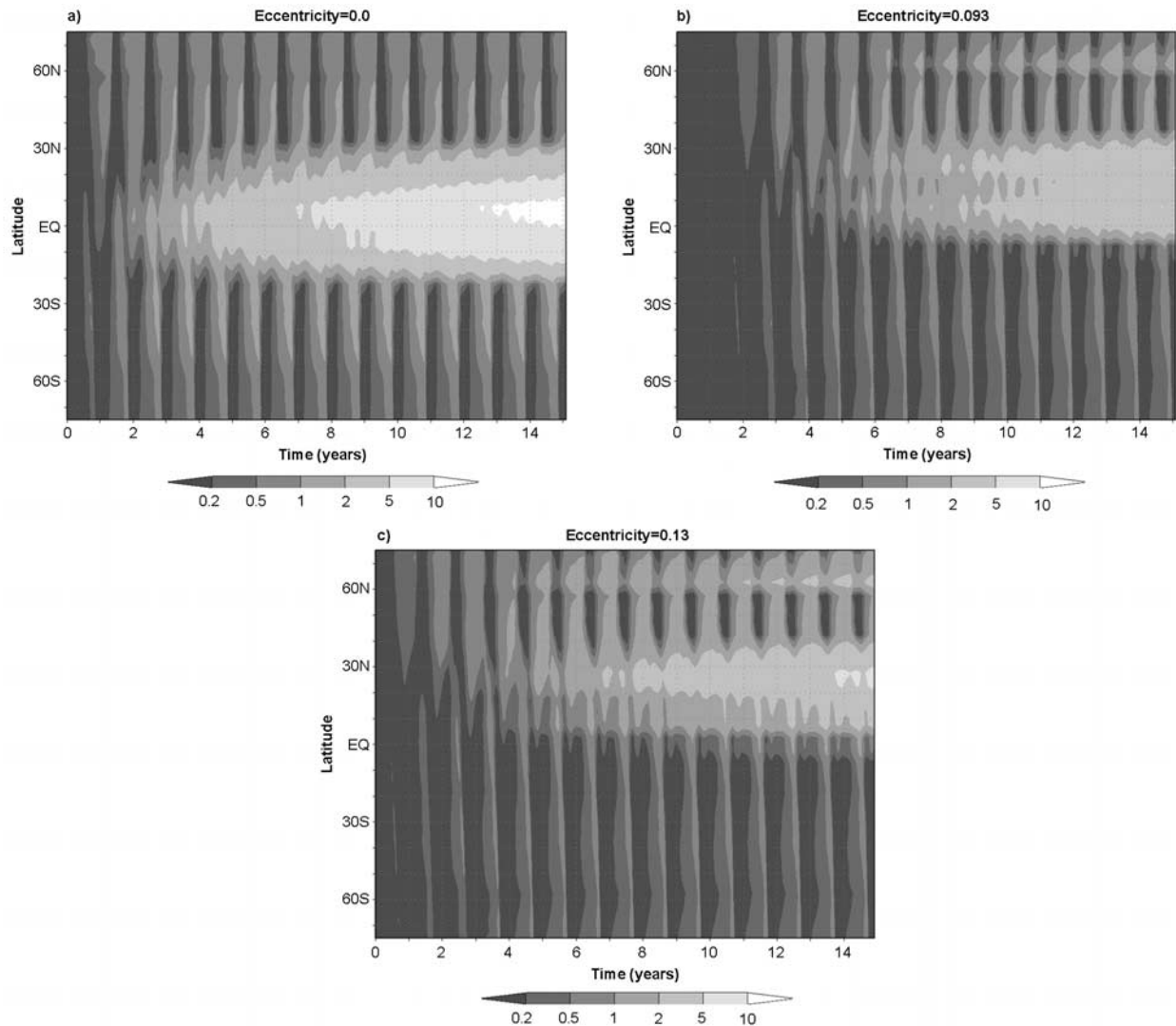


**Figure 13.** Zonally averaged surface ice abundance for full range of Martian eccentricities over  $\sim 15$  Martian years. Present-day eccentricity is (b), which is identical to Figure 7a. Ice abundance measured in cm.

expect, both the abundance and position of ice fall between the two extremes outlined above (Figure 14b).

## 6. Stability and Evolution of Water Ice

[33] In the previous section, we examined the effect of the basic orbital and spin parameters on the water cycle with a very restricted experiment design. In each case the simulations assumed a contemporary initial distribution of surface volatiles and an initial state that resulted from a lengthy spin-up of the GCM with present spin and orbital parameters. For each simulation, the parameters to be investigated were instantaneously perturbed to their new state and the model was integrated forward in time. The previous section shows some important behaviors of the system but a number of questions remain open because of the limited duration of each simulation, the intractability of integrating over complete orbital cycles, and the fixed initial distribution of volatiles. In this section, we

describe some further simulations intended to address these questions.

### 6.1. Stability of an Ice Covered Mars at High Obliquity

[34] An interesting question arising from section 5.1 is at what point ice in the tropics will equilibrate, or if the edges of this ice band will continue to creep poleward until the surface is completely ice-covered. In order to examine whether an ice covered state is viable and to examine the history dependence of the water cycle at high obliquity, we chose to attack the problem by initializing the model as a “Snowball Mars” planet, with complete ice cover. An ice layer of  $\sim 13$  cm additional thickness was placed on top of whatever ice existed at the conclusion of the s45 simulation, and the simulation was continued forward in time as s45wet.

[35] In order to provide this layer the best chance of survival (i.e., to provide a simulation that was conservative in the sense of retaining ground ice), we added code that

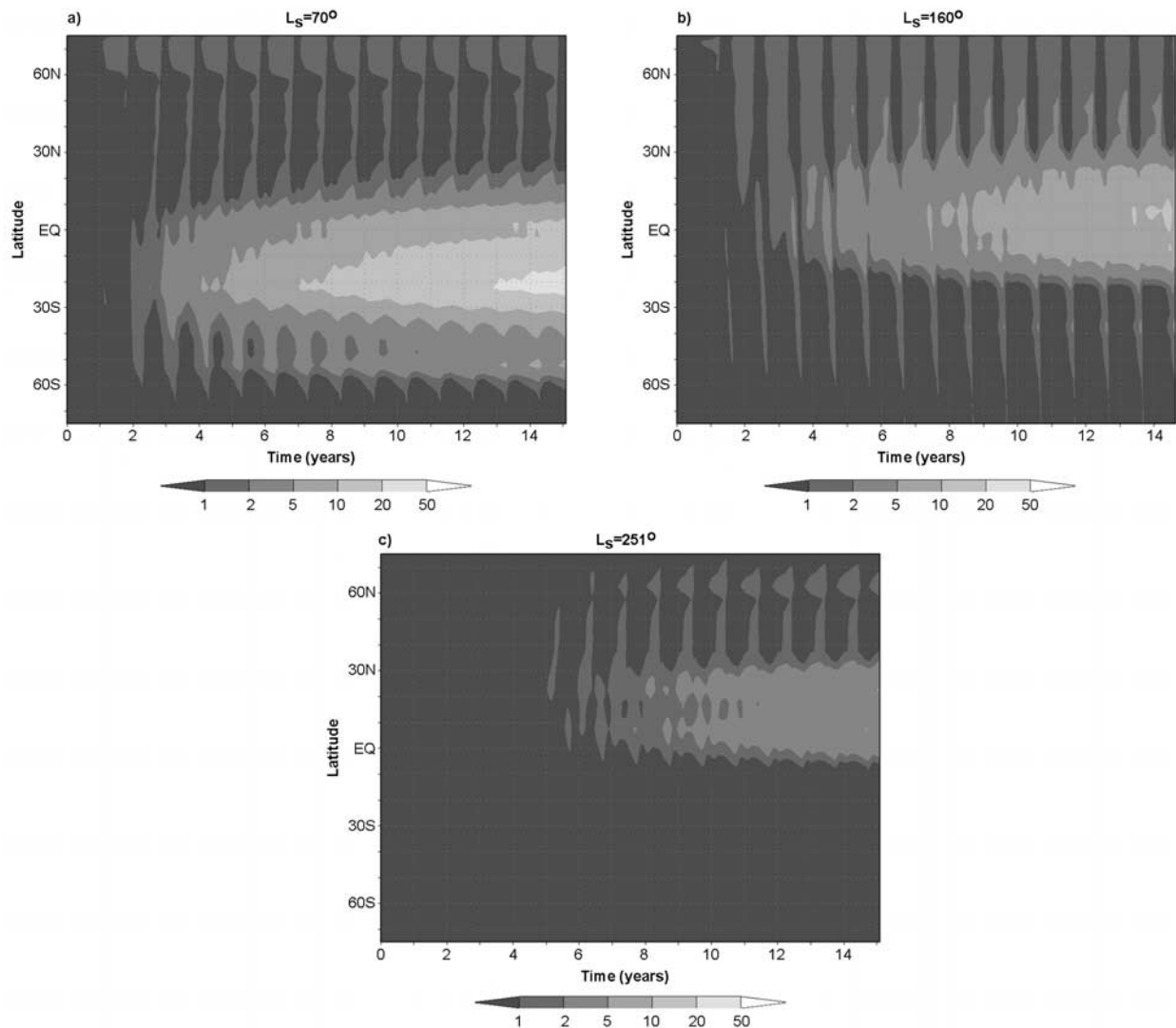


**Figure 14.** Zonally averaged surface ice abundance for varying argument of perihelion. Present-day condition is (c). Ice abundance measured in cm.

modifies (increases) the thermal inertia of a grid point when surface water ice is present. The thermal inertia is modified following *Mellon and Jakosky* [1995], whereby the conductivity of the porous regolith is replaced by that of an ice-choked regolith. A regolith porosity of 25% is assumed. This is conservative as it will tend to reduce daytime peak soil temperatures and hence increase the lifetime of a surface ice deposit (this is different from the other simulations, where, even if ice covered, the surface still retains its ice-free thermal inertia value). The results of the s45wet simulation are found in Figure 15. Quite dramatically, despite our best attempts to preserve it, all midlatitude ice has sublimated from the southern hemisphere and been transported to the equatorial band after only two years. A similar trend is evident in the northern hemisphere, albeit at a slower pace. This is further evidenced by Figure 16, which shows the atmospheric water vapor abundances over the first five years of the s45wet simulation. Note the extraordinary values in the southern cap edge during the first two years. Water is quite rapidly being lost from the south (and,

again, the north as well, though to a lesser extent) and accumulating in the tropics. What we can conclude from this is that “Snowball Mars” is not a stable configuration—all of the ice will be present either year-round in the tropics, or in the seasonal cap. The s45wet simulation suggests that the model will return to a state near that described at the end of the s45 simulation, suggesting in turn that there is only one stable state for the water model included in the current GCM, albedo and thermal inertia feedbacks notwithstanding.

## 6.2. Effect of a South Polar Water Ice Reservoir

[36] Observations of layered deposits in the southern polar region point to a more extensive reservoir of volatiles in the south at times in the past. It is worth examining such putative states when the dominant source of water ice on Mars was the southern hemisphere. The simulation s45si was initialized from a 17-year spin-up of s45, while s45p70si was initialized from a 3-year spin up of s25, with the ice being instantaneously supplanted in the southern

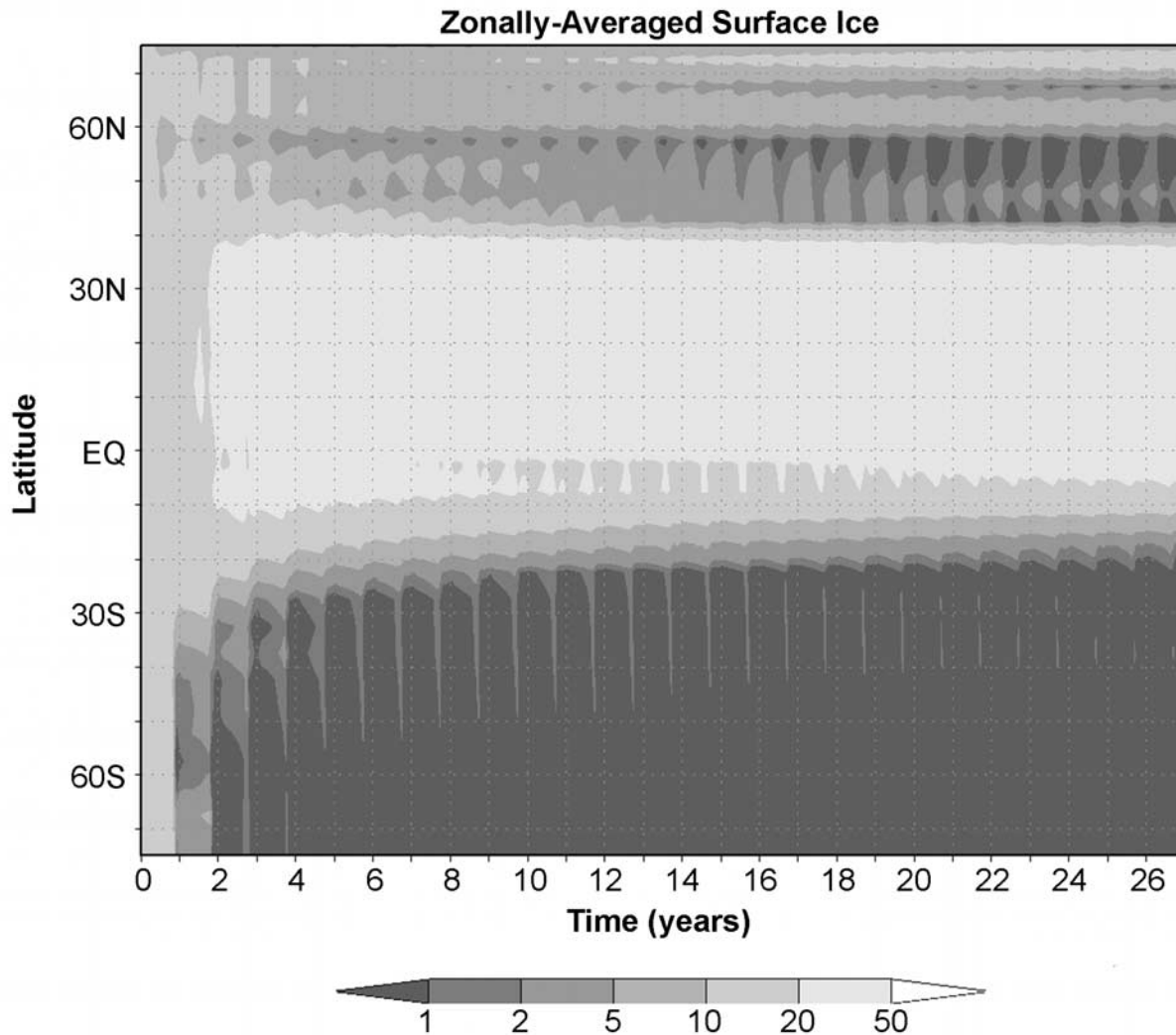


**Figure 15.** Zonally averaged surface ice for s45wet simulation. Ice abundance measured in cm. Entire surface is covered by 13 cm layer of water ice at year 0. Within two years, all midlatitude and high-latitude ice has sublimated and redeposited in the tropics.

hemisphere. The latter simulation (s45p70si) resembles s45 in that for both, the polar ice is exposed during the same season at the same position around the Sun. A comparison of the two should reveal the influence of the topographic difference between the two hemispheres on the volatile cycling. Figure 17 shows the zonally averaged surface ice for s45p70si, which should be compared with Figure 7a.

[37] The s45si simulation was run for 15 years, with the results of zonally averaged surface ice shown in Figure 18. With the water ice moved to the southern hemisphere, we now find the primary reservoir of water exposed to greater insolation (the southern hemisphere spring/summer season occurs at perihelion), and as such, we find a greater abundance of tropical ice as compared with the standard s45 case (Figure 7a). Also, a comparison with s45p70 reveals the influence of the hemispheric dichotomy (Figure 14a).

[38] This experiment also permits us to explore the extended stability of water ice in the north. With all water in the northern polar cap removed, we can trace the annual

transport of water back to the north. We do not know a priori whether ice is required to be present in the north at high obliquity. Indeed, Figure 11c suggests a fairly robust and steady depletion of ice from the northern cap. In Figure 19, we illustrate the annual cycle of water ice through the northern polar region in s45si. Within two Martian years, a full centimeter of water ice is deposited seasonally back in the north. Further exploration of this behavior is found in the following section.

### 6.3. Stability of a North Polar Ice Cap at High Obliquity

[39] We have further expanded on the results of s45si with two additional simulations intended to peg the overall stability of the northern ice cap at high obliquity. The first, s45dry, begins after a 17-year spin-up of s45 and initial removal of northern polar water ice, but without the deposition of a thick southern cap. The only reservoirs of water remaining are the atmosphere and both the tropical

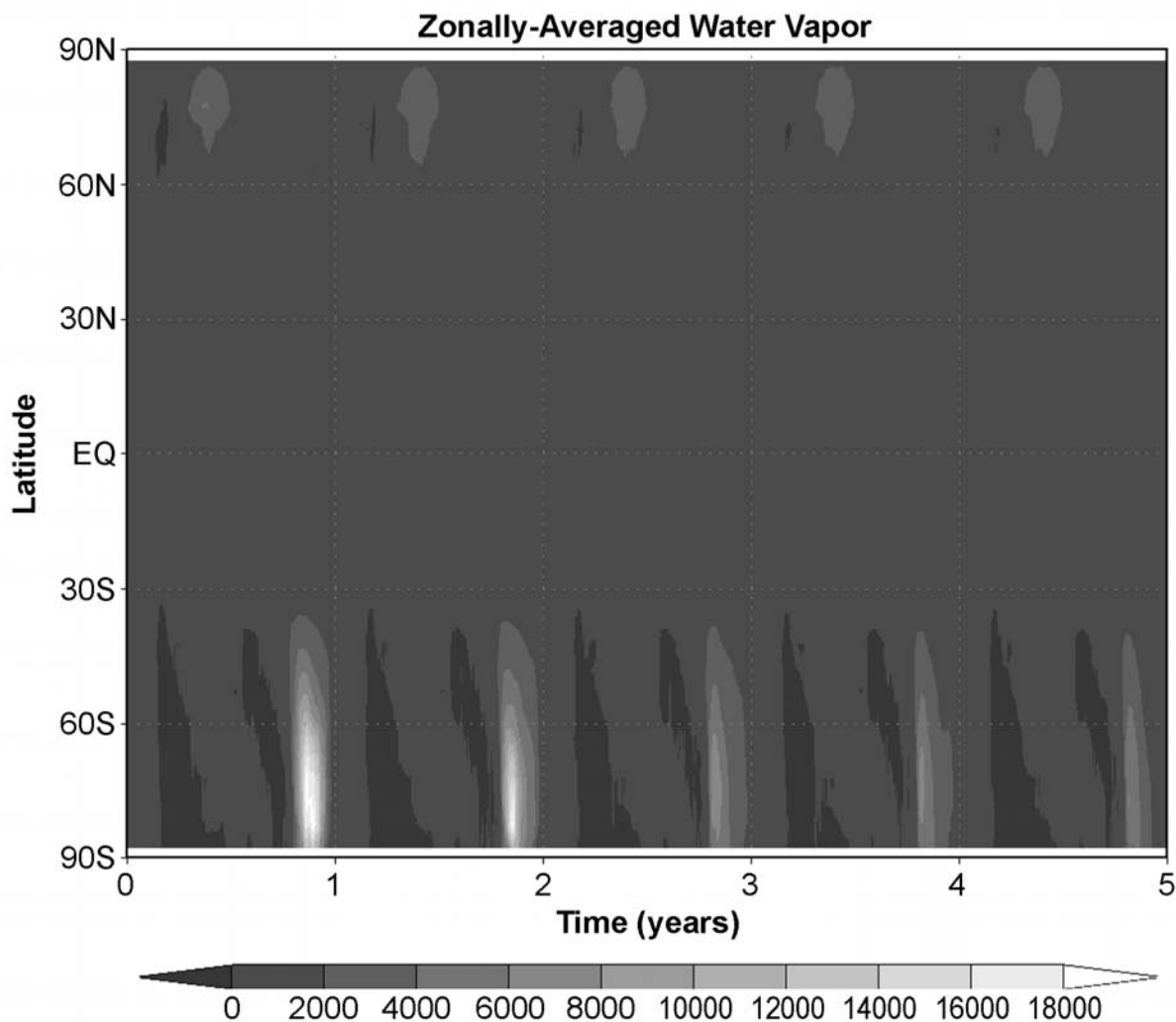


**Figure 16.** Zonally averaged water vapor abundance for first 5 years of s45wet simulation, showing extreme flux into the atmosphere during the southern summer. Water vapor abundance measured in units of pp $\mu$ m.

and south polar surface ice deposited at the conclusion of the s45 initialization. The second simulation, s45thin, also begins after a 17-year spin-up of s45, but the northern cap has been initially reduced to approximately one meter in thickness (thin enough to potentially be completely removed in only a few years). Whether any ice remains after the first few seasons will point to how much (if any) residual water will be stable in the northern polar region.

[40] Results from these simulations both point to the ultimate depletion of a residual water cap (given enough time and absent the formation of an isolating lag). Figure 20 illustrates the cap thickness at both grid points within the northern cap for both s45thin and s45dry. Approximately 15% of the remaining 1.3m of ice is lost within the first year (s45thin; Figure 20a) at 82.5°N, and depletion proceeds regularly until the cap is completely lost. At 87.5°N, depletion also occurs, but at a slower rate. If the cap is completely removed (s45dry; Figure 20b), we see at both latitude points the growth of only a thin, seasonal water ice

cap, which is quickly lost in northern spring. There does not appear to be any interannual growth of such a cap throughout the simulation. Another simulation, s35dry, performs the same experiment at 35° obliquity. Here, we see a seasonal ice cap appear every autumn at 82.5°N and burn away in the spring. At 87.5°N, however, we see the steady growth of a residual cap (Figure 21), where we saw slow depletion in s45dry. Somewhere between 35° and 45° the residual nature of the north polar cap is lost.

#### 6.4. Effect of Modeling a First-Order Obliquity Cycle

[41] Up to now, all of these results take “snapshots” in orbital time—fixing orbital and spin parameters at a single value, and observing the evolution of the system. Clearly this is not the actual behavior of Mars, and it would be ideal to simulate the precession of these parameters over their respective cycles. Doing so, however, is far beyond present computing capabilities. Presently, a yearly Martian cycle takes  $\sim$ 30 hours of CPU time on the GFDL Origin 3000

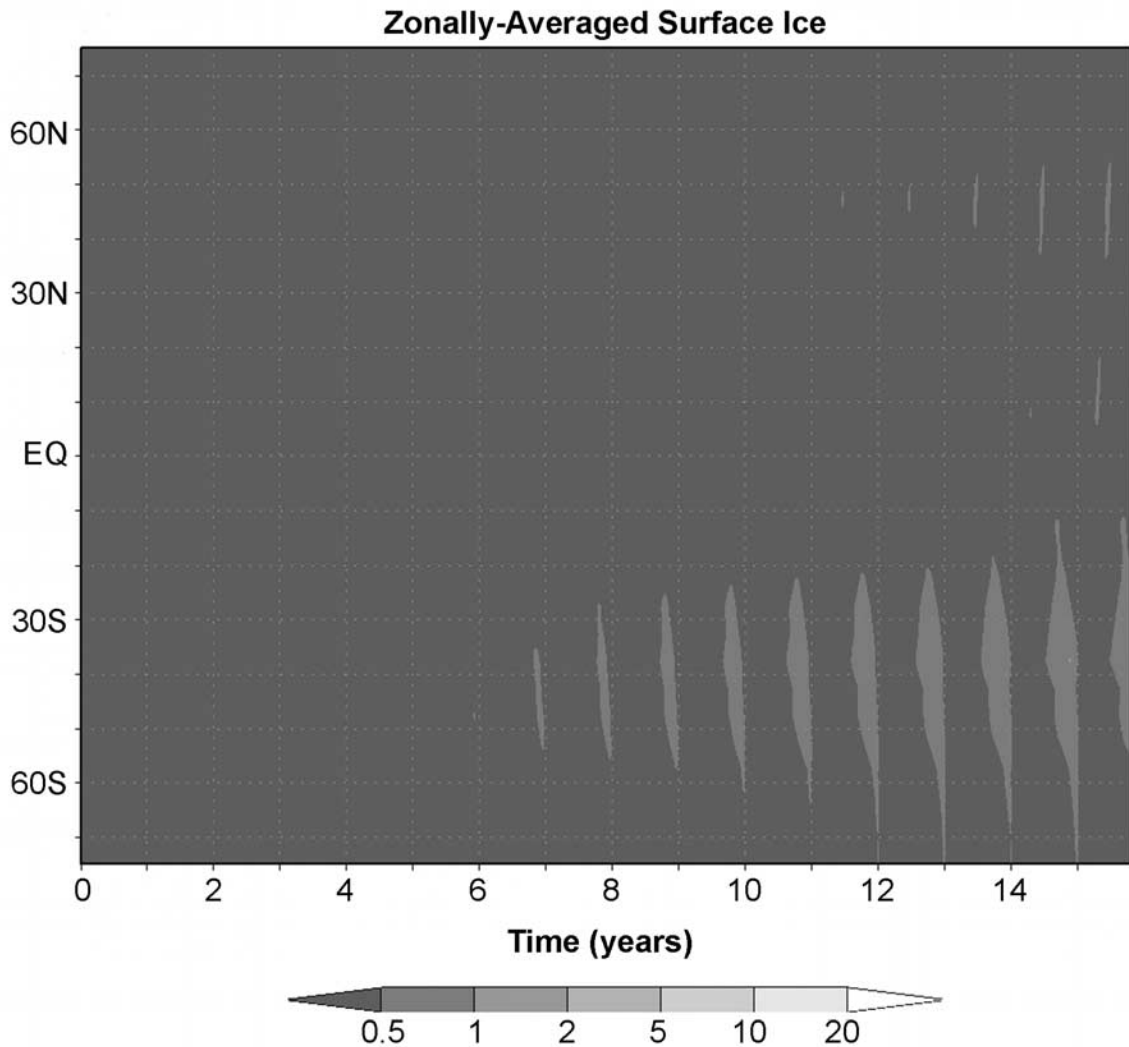


**Figure 17.** Zonally averaged surface ice for s45p70si measured in cm. Simulation s45p70si should be compared to Figure 7a (simulation s45) to appreciate the influence of the hemispheric dichotomy on climate.

supercomputer. Capturing even a single obliquity cycle of  $10^5$  years would require nearly 350 years of actual time. Because of this impracticality, we have made an attempt to simplify the problem by reducing the full obliquity cycle to its basic, binary form. The s45rev simulation starts with the s45 simulation at high ( $45^\circ$ ) obliquity for 17 Martian years, then instantaneously drops obliquity to  $25^\circ$  for an additional 27 years. Not only does this make a first-order attempt at tracing the movement of water ice over an obliquity cycle, but it also sheds light on the hysteretic nature of the climate system as a whole. At the conclusion of the s45rev simulation, we are able to compare the surface ice distribution with that of the original s25 simulation. If the final results bear little resemblance to each other, we have perhaps captured evidence that volatile distributions are not regular over orbital timescales.

[42] The results for s45rev are shown in Figure 22, which should be compared with Figure 4a. The figure shows that the system is, in fact, returning to a distribution akin to that

of present-day. The southern hemisphere has lost all residual ice deposits, and the annual progression/regression of seasonal ice has taken on a form nearly identical to s25. Slowly, the tropical and midlatitude ice is migrating northward, and being deposited on the northern cap. A similar re-emergence of the seasonal cap cycle in the north is taking place as well.

[43] The cyclic nature of these orbital states causes there to be far more potential states than those we have examined so far. Clearly, there are far too many potential conditions to make a rigorous examination tractable. Nonetheless, with some simple individual and combination simulations, we can begin to get a feel for what, if any, secular changes are expressed in the record as a result of these orbital variations.

[44] A comparison of the high obliquity surface ice map and the MOLA topography/thermal inertia data reveals a strong correlation between regions of high thermal inertia and topography, and the regions of stable surface ice. Intuitively, this makes sense, as high thermal inertia will moderate the peak daytime temperatures, making ice more

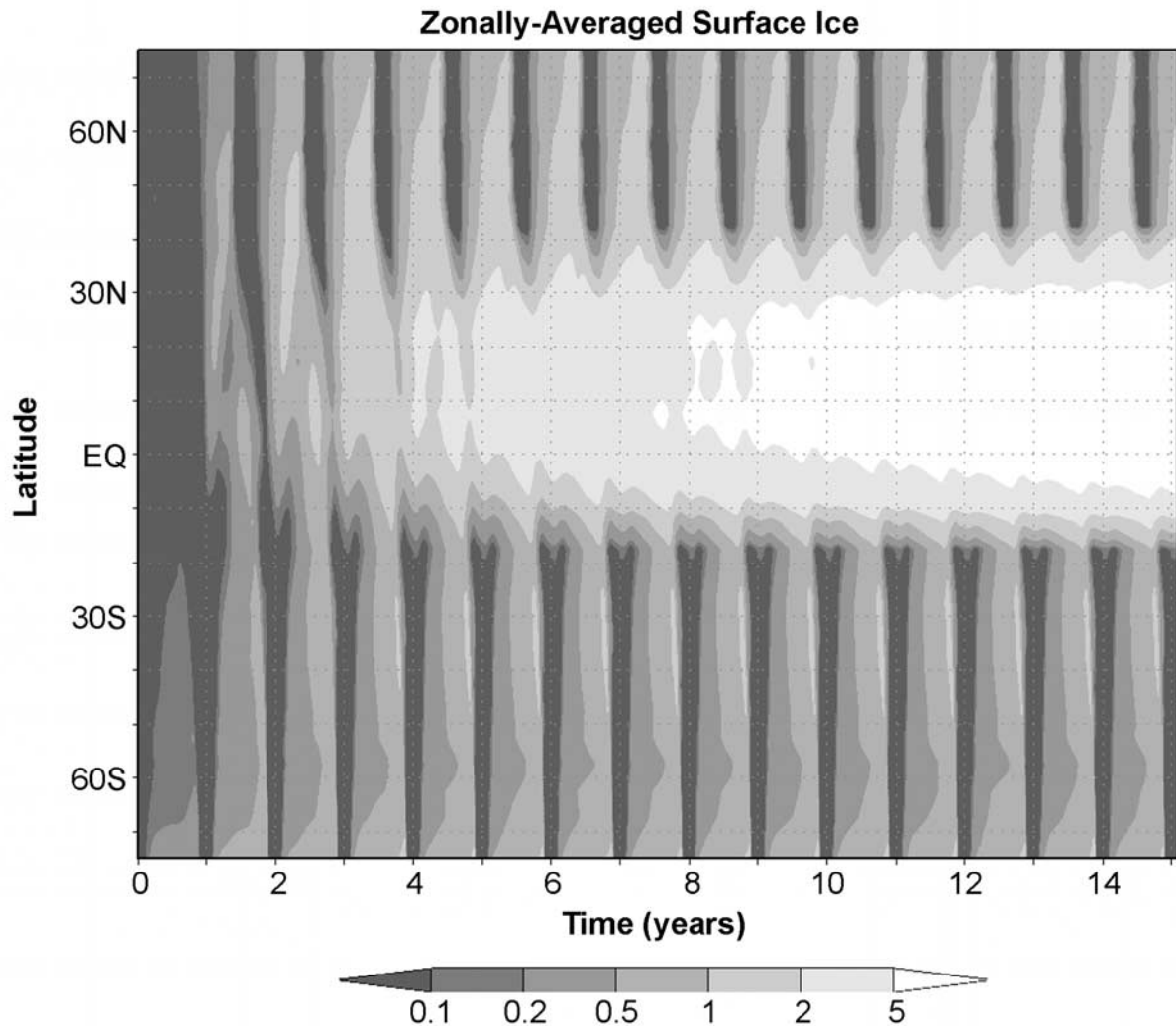


**Figure 18.** Zonally averaged surface ice for s45si simulation. Ice abundance measured in cm. North polar ice cap has been removed, and placed in southern hemisphere. Similar pattern emerges to Figure 7a. Comparison to Figure 14a reveals influence of topographic dichotomy on circulation.

able to survive through the warm daytime, as discussed in section 6.1. Also, the cooler temperatures at high altitude will be more conducive to ice retention. To validate the importance of high thermal inertia, we performed a simulation, s45smooth, where we averaged and smoothed the thermal inertia from all points in the tropics. This simulation was initialized from the 32nd year of s45 and then the thermal inertia was averaged. The result was a constant thermal inertia value across the whole tropical belt (30°N–30°S) of moderate magnitude. This would remove the high TI “peaks” where ice forms in s45, and confirm the causality between thermal inertia and ice. Indeed, this simulation reveals that by smoothing the thermal inertia, the further deposition of surface ice proceeds uniformly across longitude in the tropics.

## 7. Discussion

[45] The Mars Odyssey Gamma Ray and Neutron Spectrometer results suggest the ubiquitous presence of water

ice in the high latitudes (60°–90°) of both hemispheres [Boynton *et al.*, 2002; Feldman *et al.*, 2002; Mitrofanov *et al.*, 2002]. Further, modeling of the hydrogen content implied by the neutron and gamma ray fluxes suggests that the volume mixing ratio of ice in this region is between 40–100% ice, mixed with a lesser amount of regolith. These high volumes of water ice are difficult to interpret in terms of diffusion of water into the regolith alone [Mellon and Jakosky, 1995; Mellon *et al.*, 1997], due to the regolith porosity that would be required (Moore and Jakosky [1989] use Viking Lander data to suggest maximum porosity of surficial drift material of 60%, with blocky material having a maximum less than 50%). Modeling of the high water regions also suggests that the water rich layer is covered by a few tens of g/cm<sup>2</sup> of dry regolith [Boynton *et al.*, 2002].

[46] The work present in this paper allows a different scenario for the high water abundance regions to be developed. The model suggests that as obliquity is changed, the location of stable surface water ice will also change (see

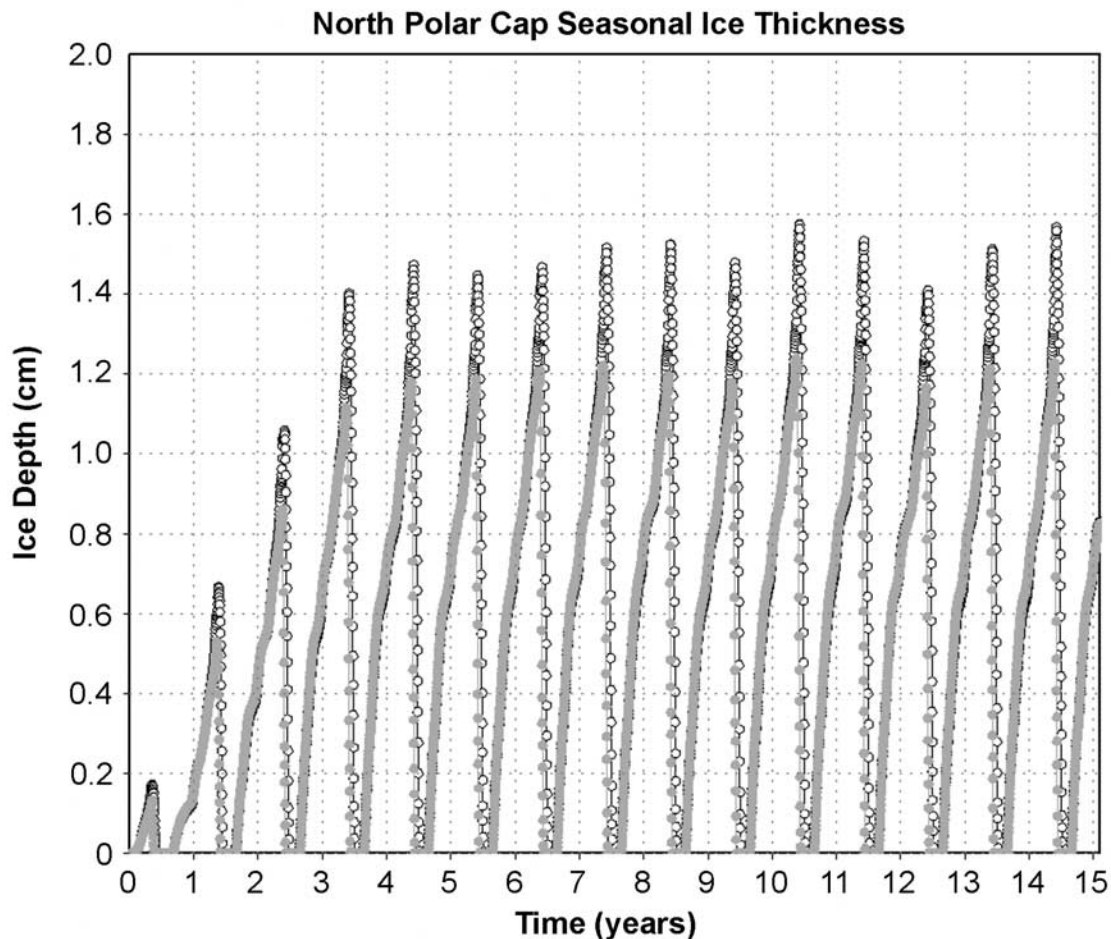


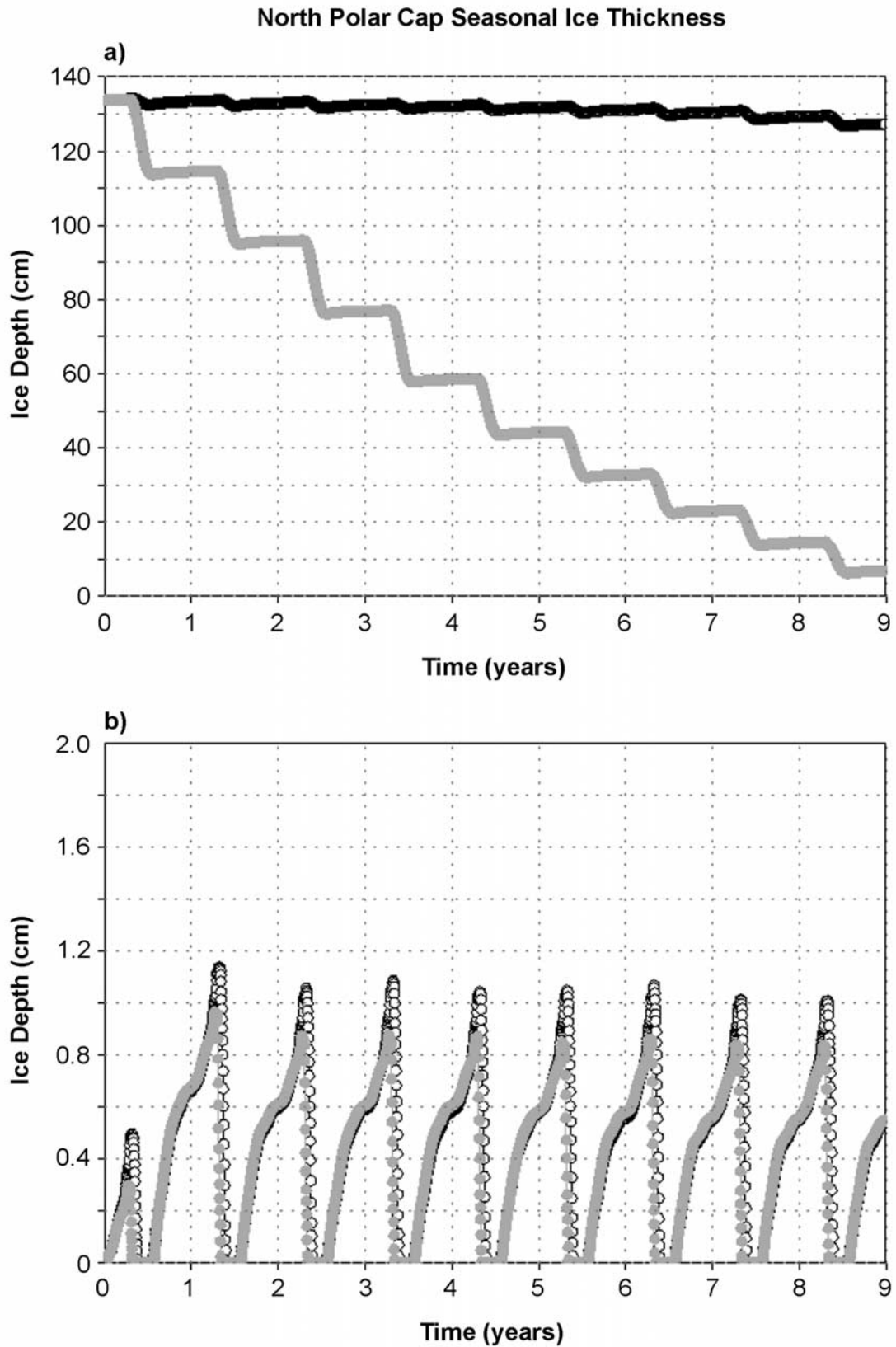
**Figure 19.** Depth of seasonal ice in cm within north polar cap for s45si simulation at 82.5°N (gray) and 87.5°N (black). Each northern winter, a centimeter of ice is deposited in the north polar region, and is quickly sublimated during northern spring.

section 5). Water will be deposited in these stable regions as an ice sheet with modest amounts of dust, as is currently believed the case for the northern residual ice cap [Kieffer, 1990]. The model currently suggests that the ice will be deposited in limited regions within the stability belt. However, this result depends sensitively upon the surface thermal properties, and it is possible that the actual distribution would be much more uniform than modeled. As obliquity moves back to lower values, the more equatorward ice becomes unstable and begins to sublimate. As these formerly stable ice sheets sublimate, the water ice component will disappear, leaving behind the atmospheric dust in the form of a surface mantle, or “lag” deposit. Over time, a progressively thicker dust lag deposit will develop as more and more ice is sublimated. Such a lag layer likely covers the southern polar layered deposits at the current orbital state [Herkenhoff and Murray, 1990; Vasavada et al., 2000]. The development of this lag will greatly reduce the rate at which water deposited at high obliquity can be returned to the poles during the subsequent low obliquity state. Thus a sufficiently thick lag deposit may preserve such surficially deposited ice sheets long after ice is no longer stable at the surface at those locations. The requirement for an upper desiccated lag layer and the very high volumetric content of

near-subsurface water ice within this scenario fits well with the GRS observations.

[47] The GRS data in the low latitudes are more ambiguous about the presence of near-surface ground ice as the lower hydrogen abundance (relative to the poles) can be interpreted as chemically bound water [Boynton et al., 2002]. However, at very high obliquity ( $>45^\circ$ ), surface ice becomes stable regionally within the tropics, and it would seem possible for a similar mechanism to leave behind much older and more deeply buried deposits of water ice.

[48] There is substantial morphological evidence for low- and midlatitude surface ice as imaged by the MOC on MGS. Wide regions of “fretted terrain” suggest the work of glacial and periglacial mechanisms. These regions include mantles pasted onto crater and canyon walls, which display viscous creep, strongly suggestive of water ice [Carr, 2001; Malin and Edgett, 2001]. Additionally, Mustard et al. [2001] present observational evidence, also from MOC, of “disaggregated terrain” in belts between 30 and 45° in both hemispheres, which they interpret as the consequence of the withdrawal of past subsurface ice. Such structures would be a natural result of the aforementioned development of a lag-covered ice sheet, but not of the formation of subsurface ice via diffusion of vapor into regolith pore spaces. Lastly,



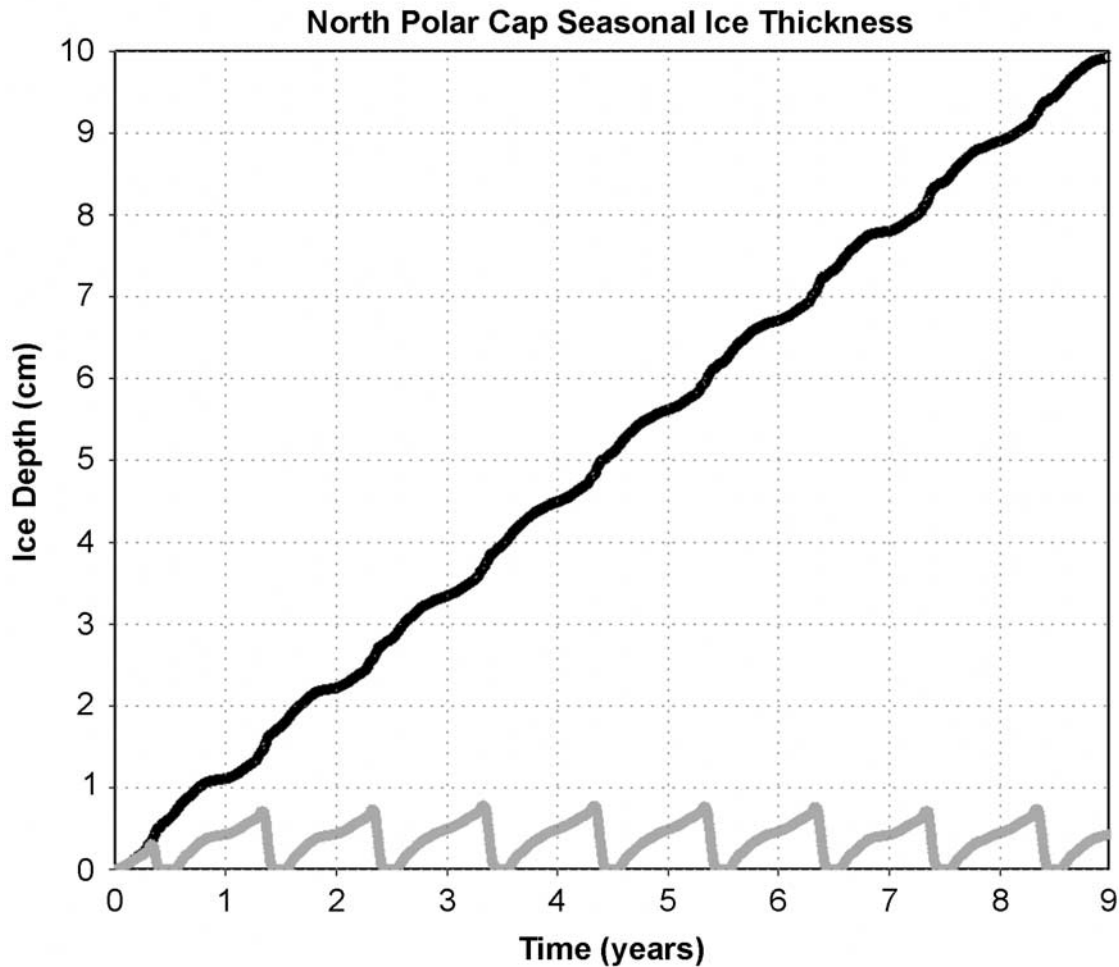


**Figure 21.** Depth of seasonal ice in cm within north polar region for s35dry simulation. In contrast to Figure 20, ice is stable and increasing in depth at 87.5°N.

*Kreslavsky and Head* [2000, 2002] have interpreted the unusual kilometer-scale roughness of the surface to imply a meters-thick, water ice-rich mantle covering nearly one-quarter of the planet.

[49] The model suggests a range of obliquities for which the northern residual polar cap is not stable. Presumably at these obliquities, substantial amounts of water ice are lost from the cap. For the reasons discussed above, however, sublimation of the northern cap is unlikely to proceed to exhaustion. The dust content of the residual cap is also likely to generate an isolating mantle, presumably as has occurred for the southern PLD. Subsequently, at low obliquity, a fresh layer of ice is deposited upon the residual lag, and ostensibly remains throughout the low obliquity period. Over numerous cycles, this can generate ice-rich and dust-rich layers [*Thomas et al.*, 1992; *Laskar et al.*, 2002].

[50] Our computational results confirm the ability of water ice to move across the entire planet, and also provide a clean mechanism for distributing this ice over many timescales. Our simulations (section 5) reveal that the initial transport of exposed surface ice will proceed fairly rapidly with the obliquity cycle. Once emplaced, by simply mantling the surface ice with dust, one can retain it over time-

scales substantially longer than those required for its emplacement. This presents the opportunity to develop layering and layered deposits of ice and lag, similar to the PLD, at any latitude on the planet.

## 8. Summary

[51] We have investigated the cycles of water vapor and carbon dioxide as a function of orbital elements, using the GFDL Mars GCM. The model includes a full description of exchange between surface ice and atmospheric water, transport of water in the atmosphere and cloud formation. The model does not include radiative feedbacks due to water vapor and clouds that would be important at high obliquity. It also does not include subsurface storage or diffusion of H<sub>2</sub>O and CO<sub>2</sub>. However, this model represents a significant improvement over previous models through its self-consistent treatment of atmospheric water vapor transport. The results capture the first-order behavior of the volatile cycles. The following conclusions can be drawn from this work:

[52] 1. The atmospheric surface pressure cycle is more extreme at high obliquity. Assuming no exchange with the long-term regolith CO<sub>2</sub> reservoir, the pressure maxima

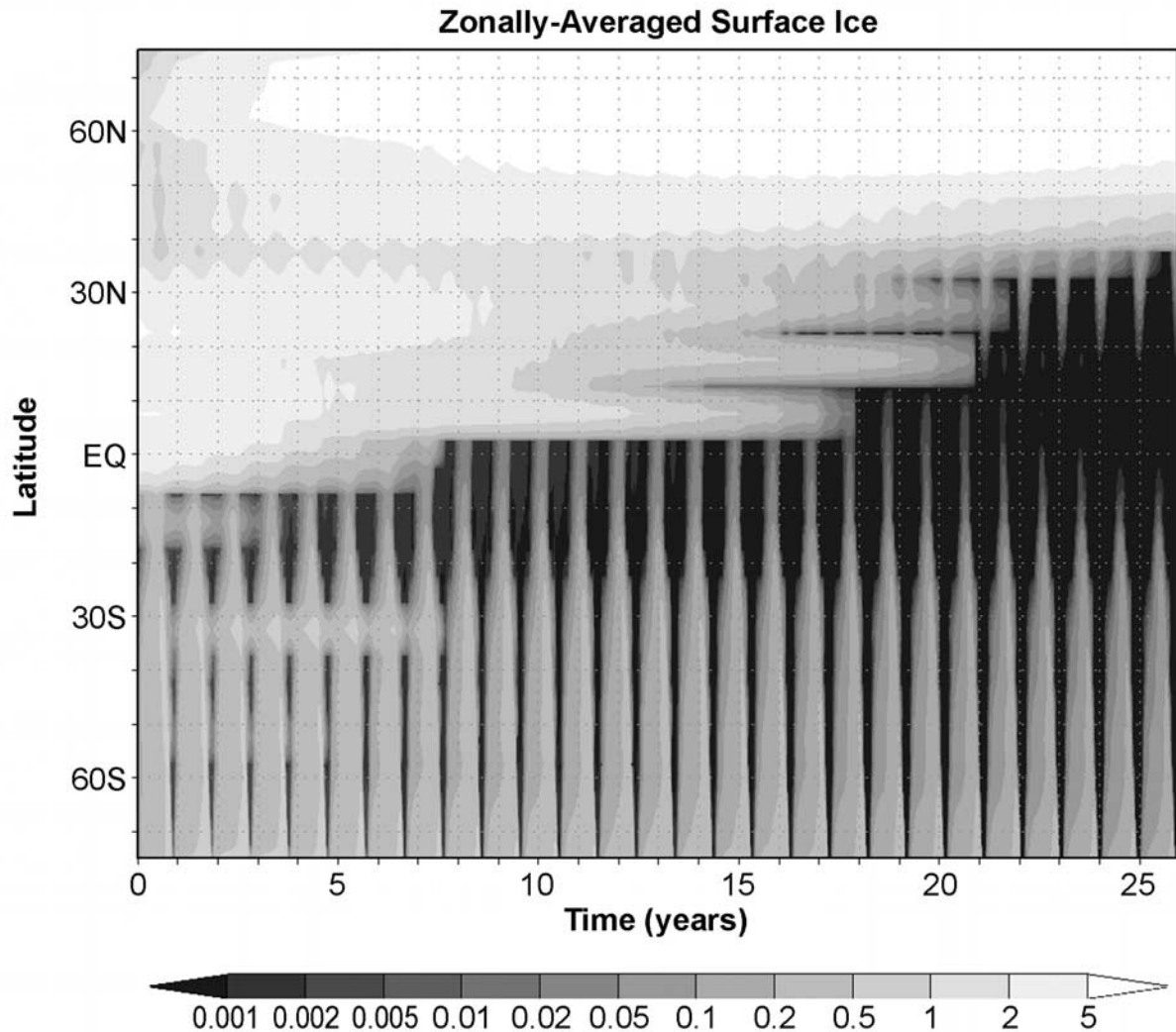


**Figure 22.** Zonally averaged surface ice for s45rev simulation. Ice abundance measured in cm. At year zero, obliquity is switched from 45° to 25°, and surface ice movement is observed. Fairly rapidly (on orbital timescales), ice returns to its original 25° configuration (seen in Figure 4a). Seasonal ice caps in both hemispheres have emerged.

do not appreciably change, while the wintertime minima decrease substantially. This results from the greater fraction of the planet consumed by polar night during winter.

[53] 2. Increasing planetary obliquity increases the quantity of water vapor in the atmosphere and the abundance of water ice clouds, as the polar caps are exposed to greater insolation. The region of stable surface ice migrates equatorward with increasing obliquity. At 35°, surface ice is stable in the high midlatitudes. At 45° and above, surface ice is stable in tropical latitudes, although the exact position is biased toward the hemisphere with aphelion summer.

[54] 3. At high obliquity, ice is not uniformly stable at a given latitude, but preferentially deposited in regions of high topography and/or high thermal inertia.

[55] 4. Eccentricity and argument of perihelion enhance the vigor of the water cycle and the abundance of deposited surface ice by modifying the polar insolation, especially at high obliquity.

[56] 5. Several hysteresis experiments indicate that the location and stability of surface ice is quite repetitive over orbital cycles and is most closely linked to obliquity.

[57] **Acknowledgments.** The authors would like to thank Bruce Jakosky and one anonymous reviewer for their thoughtful comments. This work was funded by Mars Fundamental Research Program grant #NAG5-12915. Many thanks to Jim Garvin for making this work possible.

## References

- Boynton, W. V., et al., Distribution of hydrogen in the near surface of Mars: Evidence for subsurface ice deposits, *Science*, 297, 81–85, 2002.
- Briggs, G. A., The nature of the residual Martian polar caps, *Icarus*, 23, 167–191, 1974.
- Carr, M. H., Mars Global Surveyor observations of Martian fretted terrain, *J. Geophys. Res.*, 106, 23,571–23,594, 2001.
- Feldman, W. C., et al., Global distribution of neutrons from Mars: Results from Mars Odyssey, *Science*, 297, 75–78, 2002.
- François, L. M., J. C. G. Walker, and W. R. Kuhn, A numerical simulation of climate changes during the obliquity cycle on Mars, *J. Geophys. Res.*, 95, 14,761–14,778, 1990.

- Haberle, R. M., and B. M. Jakosky, Sublimation and transport of water from the north residual polar cap on Mars, *J. Geophys. Res.*, *95*, 1423–1437, 1990.
- Haberle, R. M., J. R. Murphy, and J. Schaeffer, Orbital change experiments with a Mars general circulation model, *Icarus*, *161*, 66–89, 2003.
- Herkenhoff, K. E., and B. C. Murray, Color and albedo of the south polar layered deposits on Mars, *J. Geophys. Res.*, *95*, 14,511–14,529, 1990.
- Hess, S., L. Henry, and R. M. Tillman, The seasonal variation of atmospheric pressure on Mars as affected by the south polar cap, *J. Geophys. Res.*, *84*, 2923–2927, 1979.
- Hess, S. L., J. A. Ryan, J. E. Tillman, R. M. Henry, and C. B. Leovy, The annual cycle of pressure on Mars measured by Viking Landers 1 and 2, *Geophys. Res. Lett.*, *7*, 197–200, 1980.
- Hourdin, F., P. Le Van, F. Forget, and O. Talagrand, Meteorological variability and the annual surface pressure cycle on Mars, *J. Atmos. Sci.*, *50*, 3625–3640, 1993.
- Jakosky, B. M., The role of seasonal reservoirs in the Mars water cycle. I. Seasonal exchange of water with the regolith, *Icarus*, *55*, 1–18, 1983a.
- Jakosky, B. M., The role of seasonal reservoirs in the Mars water cycle. II. Coupled models of the regolith, the polar caps, and atmospheric transport, *Icarus*, *55*, 19–39, 1983b.
- Jakosky, B. M., and M. H. Carr, Possible precipitation of ice at low latitudes of Mars during periods of high obliquity, *Nature*, *315*, 559–561, 1985.
- Jakosky, B., M. Henderson, and B. G. Mellon, The Mars water cycle at other epochs—Recent history of the polar caps and layered terrain, *Icarus*, *102*, 286–297, 1993.
- Jakosky, B. M., B. G. Henderson, and M. T. Mellon, Chaotic obliquity and the nature of the Martian climate, *J. Geophys. Res.*, *100*, 1579–1584, 1995.
- Kieffer, H. H., H<sub>2</sub>O grain size and the amount of dust in Mars' residual north polar cap, *J. Geophys. Res.*, *95*, 1481–1493, 1990.
- Kreslavsky, M. A., and J. W. Head III, Kilometer-scale roughness of Mars: Results from MOLA data analysis, *J. Geophys. Res.*, *105*, 26,695–26,711, 2000.
- Kreslavsky, M. A., and J. W. Head III, Mars: Nature and evolution of young latitude-dependent water-ice-rich mantle, *Geophys. Res. Lett.*, *29*(15), 1904, doi:10.1029/2002GL015392, 2002.
- Laskar, J., and P. Robutel, The chaotic obliquity of the planets, *Nature*, *361*, 608–612, 1993.
- Laskar, J., B. Levrard, and J. F. Mustard, Orbital forcing of the Martian polar layered deposits, *Nature*, *419*, 375–377, 2002.
- Leighton, R. B., and B. C. Murray, Behavior of carbon dioxide and other volatiles on Mars, *Science*, *153*, 136–144, 1966.
- Malin, M. C., and K. S. Edgett, Mars Global Surveyor Mars Orbiter Camera: Interplanetary cruise through primary mission, *J. Geophys. Res.*, *106*, 23,429–23,570, 2001.
- Mellon, M. T., and B. M. Jakosky, The distribution and behavior of Martian ground ice during past and present epochs, *J. Geophys. Res.*, *100*, 11,781–11,799, 1995.
- Mellon, M., T. Jakosky, and B. M. Postawko, The persistence of equatorial ground ice on Mars, *J. Geophys. Res.*, *102*, 19,357–19,370, 1997.
- Mitrofanov, I., et al., Maps of subsurface hydrogen from the High Energy Neutron Detector, Mars Odyssey, *Science*, *297*, 78–81, 2002.
- Moore, H. J., and B. M. Jakosky, Viking landing sites, remote-sensing observations, and physical properties of Martian surface materials, *Icarus*, *81*, 164–184, 1989.
- Mustard, J. F., C. D. Cooper, and M. K. Rifkin, Evidence for recent climate change on Mars from the identification of youthful near-surface ground ice, *Nature*, *412*, 411–414, 2001.
- Palluconi, F. D., and H. H. Kieffer, Thermal inertia mapping of Mars from 60°S to 60°N, *Icarus*, *45*, 415–426, 1981.
- Pleskot, L. K., and E. D. Miner, Time variability of Martian bolometric albedo, *Icarus*, *45*, 179–201, 1981.
- Pollack, J. B., C. B. Leovy, Y. H. Mintz, and W. Van Camp, Winds on Mars during the Viking season: Predictions based on a general circulation model with topography, *Geophys. Res. Lett.*, *3*, 479–482, 1976.
- Pollack, J. B., C. B. Leovy, P. W. Greiman, and Y. Mintz, A Martian general circulation experiment with large topography, *J. Atmos. Sci.*, *38*, 3–29, 1981.
- Pollack, J. B., R. M. Haberle, J. Schaeffer, and H. Lee, Simulations of the general circulation of the Martian atmosphere I. Polar processes, *J. Geophys. Res.*, *95*, 1447–1473, 1990.
- Pollack, J. B., R. M. Haberle, J. R. Murphy, J. Schaeffer, and H. Lee, Simulations of the general circulation of the Martian atmosphere, 2. Seasonal pressure variations, *J. Geophys. Res.*, *98*, 3149–3181, 1993.
- Richardson, M. I., and R. J. Wilson, Investigation of the nature and stability of the Martian seasonal water cycle with a general circulation model, *J. Geophys. Res.*, *107*(E5), 5031, doi:10.1029/2001JE001536, 2002a.
- Richardson, M. I., and R. J. Wilson, A topographically forced asymmetry in the Martian circulation and climate, *Nature*, *416*, 298–301, 2002b.
- Richardson, M. I., R. J. Wilson, and A. V. Rodin, Water ice clouds in the Martian atmosphere: General circulation model experiments with a simple cloud scheme, *J. Geophys. Res.*, *107*(E9), 5064, doi:10.1029/2001JE001804, 2002.
- Thomas, P., S. W. Squyres, K. Herkenhoff, A. Howard, and B. Murray, Polar deposits of Mars, in *Mars*, edited by H. H. Kieffer et al., pp. 767–798, Univ. of Ariz. Press, Tucson, 1992.
- Tillman, J. E., Mars global atmospheric oscillations: Annually synchronized, transient normal-mode oscillations and the triggering of global dust storms, *J. Geophys. Res.*, *93*, 9433–9451, 1988.
- Touma, J., and J. Wisdom, The chaotic obliquity of Mars, *Science*, *259*, 1294–1296, 1993.
- Vasavada, A. R., J. P. Williams, D. A. Paige, K. E. Herkenhoff, N. T. Bridges, R. Greeley, B. C. Murray, D. S. Bass, and K. S. McBride, Surface properties of Mars' polar layered deposits and polar landing sites, *J. Geophys. Res.*, *105*, 6961–6970, 2000.
- Ward, W. R., and D. J. Rudy, Resonant obliquity of Mars?, *Icarus*, *94*, 160–164, 1992.
- Wilson, R. J., A general circulation model simulation of the Martian polar warming, *Geophys. Res. Lett.*, *24*, 123–127, 1997.
- Wilson, R. J., and K. P. Hamilton, Comprehensive model simulation of thermal tides in the Martian atmosphere, *J. Atmos. Sci.*, *53*, 1290–1326, 1996.
- Wilson, R. J., and M. I. Richardson, The Martian atmosphere during the Viking mission, I. Infrared measurements of atmospheric temperatures revisited, *Icarus*, *145*, 555–579, 2000.

D. J. McCleese, Jet Propulsion Laboratory, 4800 Oak Grove Drive, Pasadena, CA 91109, USA.

M. A. Mischna, Department of Earth and Space Sciences, University of California, Los Angeles, 595 Charles Young Drive East, Los Angeles, CA 90095, USA. (mischna@ucla.edu)

M. I. Richardson, Division of Geological and Planetary Sciences, California Institute of Technology, MS 150-21, Pasadena, CA 91125, USA. (mir@gps.caltech.edu)

R. J. Wilson, Geophysical Fluid Dynamics Laboratory, Princeton, NJ 08540, USA.